P148381.PDF [Page: 3 of 87]

93-636

COMMUNICATIONS
RESEARCH
LABORATORY

MULTIPATH MEASUREMENT AND MODELLING

by

J. Litva
and
L. Lai

Final Report for
Defence Research Establishment Ottawa
Under Contract no. W7714-1-9507

Faculty of Engineering
McMaster University
Hamilton, Ontario
Canada L8S 4K1

CRL Report No. 255
July 1992

P148381.PDF [Page: 5 of 87]

105-03443/

MULTIPATH MEASUREMENT AND MODELLING

by

J. Litva
and
L. Lai

CRL Report No. 255
July 1992

P148381.PDF [Page: 7 of 87]

MULTIPATH MEASUREMENT AND MODELLING

J. Litva and L. Lai

Communications Research Laboratory

McMaster University, Hamilton, Ontario, Canada

Final report for

Defence Research Establishment Ottawa

~~Under Contract No.: 3-53685~~

Date of Report: September 1992

P148381.PDF [Page: 9 of 87]

Acknowledgments

The authors would like to express their gratitude to Mr. T. Lo of the CRL for his continuous help and for all those helpful discussions and suggestions in the preparation and ongoing of this project. Most of the experiments in this project would not have been completed without his participation. The authors are also in debted to Mr. William Read of the DREO for his forbearance on the delay of the project. His guidance during the field measurement is the most appreciated. Further thanks are extended to Mr. R. Fines, Mr. J. Caseault, Mr. M. Stoffels, and Mr. P. Okulich of the Applied Silicon Inc. Canada for their efforts that spent on the system and making it work.

TABLE OF CONTENTS

		page
Acknowledgments		ii
TABLE OF CONTENTS		iii
LIST OF FIGURES		v
GLOSSARY		viii
1.	INTRODUCTION	1
2.	PMMS SYSTEM SPECIFICATIONS	3
2.1	General Description	3
2.2	System Upgrade	3
2.3	Data Acquisition	4
2.4	System Calibration	6
3.	SIGNAL MODEL	7
4.	CALIBRATION TECHNIQUES	11
4.1	Ho's Array Calibration Algorithm	11
4.2	Friedlander - Weiss's Self Calibration Algorithm	14
4.3	Calibration Based on Experimental Reference Data	17
5.	DATA ANALYSIS	18
5.1	System Calibration	18
5.2	Single Source Measurements	19
5.3	Two Sources Measurements	19
5.4	Measurements in the Proximity of a Fence	20

P148381.PDF [Page: 11 of 87]

6. CONCLUSIONS AND FUTURE WORK 23

Reference 26

Appendix 1 27

Figures 29

LIST OF FIGURES

Figure 1.1 A linear array rests on a fibreglass platform.

Figure 1.2 Another view of the linear array and its platform.

Figure 2.1 A block diagram of the multipath measurement system.

Figure 2.2 A schematic diagram of an IF channel of the multipath measurement system.

Figure 2.3 The data acquisition unit of the multipath measurement system.

Figure 3.1 Geometry of a linear array, showing a ray of an incident plane wave.

Figure 4.1 Simulation results based on Ho's calibration algorithm.
The input parameters were DOA=(-10°, 5°), gain variance σ_α=0.5, phase variance σ_ψ=20°, SNR=30dB.
(a) Spatial spectrum after iterations 1, 2, 4, and 6.
(b) The convergence of the least-square norm after each iteration.
(c) The estimated gain after each iteration.
(d) The estimated phase after each iteration.

Figure 4.2 Simulation results based on Ho's calibration algorithm.
The input parameters were DOA=(-5°, 3°), gain variance σ_α=0.5, phase variance σ_ψ=20°, SNR=20 dB.
(a) Spatial spectrum after iterations 1, 2, 7, and 15.
(b) The convergence of the least-square norm after each iteration.
(c) The estimated gain after each iteration.
(d) The estimated phase after each iteration.

Figure 4.3 Simulation results based on Friedlander and Weiss's calibration algorithm.
The input parameters were DOA=(-30°, -5°, 35°), gain variance σ_α=0.2, phase variance σ_ψ=20°, SNR=20 dB.
(a) Spatial spectrum after iterations 1, 2, and 4.
(b) The convergence of the cost function after each iteration.
(c) The estimated gain after each iteration.
(d) The estimated phase after each iteration.

Figure 4.4 Simulation results based on Friedlander and Weiss's calibration algorithm. The input parameters were DOA=(-30°, -5°, 35°), gain variance σ_α=0.5, phase variance σ_ψ=40°, SNR=30 dB.
(a) Spatial spectrum after iterations 1, 2, 3, and 6.
(b) The convergence of the cost function after each iteration.
(c) The estimated gain after each iteration.
(d) The estimated phase after each iteration.

Figure 5.1 A site survey on bearing measurement using a theodolite.

Figure 5.2 A site survey based on tape measurement.

Figure 5.3 System calibration carried out on April 28 am, 1992.
(a) Gain characteristics due to various signal attenuation.
(b) Phase characteristics due to various signal attenuation.
(c) Magnitude of the dc offset value.
(d) Phase of the dc offset value.

Figure 5.4 System calibration carried out on April 28 pm, 1992.
(a) Gain characteristics due to various signal attenuation.
(b) Phase characteristics due to various signal attenuation.
(c) Magnitude of the dc offset value.
(d) Phase of the dc offset value.

Figure 5.5 System calibration carried out on April 29, 1992.
(a) Gain characteristics due to various signal attenuation.
(b) Phase characteristics due to various signal attenuation.
(c) Magnitude of the dc offset value.
(d) Phase of the dc offset value.

Figure 5.6 FFT beamforming with source at L3, i.e., 13.6° left of the array boresight.
(a) Beam pattern
(b) Beam pattern with channel gain imbalance and dc offset removed.

Figure 5.7 FFT beamforming with source at L2, i.e., 9.2° left of the array boresight.
(a) Beam pattern
(b) Beam pattern with channel gain imbalance and dc offset removed.

Figure 5.8 FFT beamforming with source at L1, i.e., 4.6° left of the array boresight.
(a) Beam pattern
(b) Beam pattern with channel gain imbalance and dc offset removed.

Figure 5.9 FFT beamforming with source at R1, i.e., 4.6° right of the array boresight.
(a) Beam pattern
(b) Beam pattern with channel gain imbalance and dc offset removed.

Figure 5.10 FFT beamforming with source at R2, i.e., 9.2° right of the array boresight.
(a) Beam pattern
(b) Beam pattern with channel gain imbalance and dc offset removed.

Figure 5.11 FFT beamforming with source at R3, i.e., 13.75° right of the array boresight.
(a) Beam pattern
(b) Beam pattern with channel gain imbalance and dc offset removed.

Figure 5.12 FFT beamforming with source at R4, i.e., 18° right of the array boresight.
(a) Beam pattern
(b) Beam pattern with channel gain imbalance and dc offset removed.

Figure 5.13 Direction of arrival estimation on real data using Friedlander and Weiss's calibration algorithm.

Figure 5.14 FFT beamforming on two coherent sources. Sources were at -9.2° and 0°.
(a) Beam pattern
(b) Beam pattern with channel gain imbalance and dc offset removed

Figure 5.15 FFT beamforming on two coherent sources. Sources were at -13.6° and 0°.
(a) Beam pattern
(b) Beam pattern with channel gain imbalance and dc offset removed.

Figure 5.16 FFT beamforming pattern with the presence of a poultry fence.
The source was at -4.6° with respect to the array boresight.

Figure 5.17 FFT beamforming pattern with the presence of a poultry fence.
The source was at 9.2° with respect to the array boresight.

Figure 5.18 Glint for the two-element target [6].

GLOSSARY

Principal Symbols

$a(\theta_n)$	steering vector
A	a matrix of N steering vectors
c	wave propagation velocity
d	interelement spacing of an array
f_c	carrier frequency
G	a diagonal matrix of gain-phase uncertainty of the array elements
G(k)	antenna gain for the *kth* snapshot
G_m	gain and phase of the *mth* element
i	index of minimization iterations
I	identity matrix
J_c	cost function
k	ratio of amplitude of target 2 to target 1
K	number of samples
M	number of sensor
N	number of incident wave
$P^{(i)}(\theta)$	spectral spectrum for the *ith* iteration
$Q(\theta_n)$	diagonal matrix whose elements are steering vector
R_s	covariance matrix of the signal
R_x	covariance matrix of the array output vector
S(k)	baseband signal vector for the *kth* snapshot

P148381.PDF [Page: 16 of 87]

S_n	baseband signal vector due to the *nth* radiated signal
$V(k)$	noise vector at the array for the *kth* snapshot
V_m	noise vector at the *mth* element
$X(k)$	signal vector received at the array for the *kth* snapshot
X_m	signal vector at the *mth* element
u_i	eigenvectors
U	noise subspace
U_L	left singular vector
U_R	right singular vector
U_{RM}	*Mth* column of the right singular vector
α_m	magnitude of the antenna gain
β_m	singular values from singular value decomposition
χ	glint error
γ	relative phase angle
γ_m	uniformly distributed random number between 0 and 1
δ	a vector of gain imbalance
λ	wavelength
λ_i	eigenvalues
Λ	diagonal matrix of singular values
μ	least-square norm
ψ_m	phase of the antenna gain
σ_n	average noise power

σ_s	signal power
σ_α	variance of the sensor gain magnitude
σ_ψ	variance of the sensor phase
θ_n	angle of arrival of the n*th* wavefront
φ_n	phase angle due to the n*th* radiated signal
ζ_m	uniformly distributed random number between 0 and 1

Mathematical Operation

$(\cdot)^T$	transpose
$(\cdot)^H$	Hermitian transpose
$E\{\cdot\}$	mathematical expectation
$(\cdot)^{-1}$	inverse
$\hat{Y}$	an estimated value of Y

Abbreviations

A/D	analogue to digital
dc	direct current
DOA	direction of arrival
I	in-phase component
IF	intermediate frequency
LO	local oscillator
MHz	mega hertz = 10^6 cycles per second
MUSIC	multiple signal characterization

Q	quadrature component
RF	radio frequency
SNR	signal to noise ratio
SVD	singular value decomposition
TX	transmitter
VHF	very high frequency

1. INTRODUCTION

It has been observed that whenever multipath signals are a component in the signal environments of most receiving systems that their performance is severely degraded. This is particularly true of radio direction finding (DF) systems. It is now commonly believed that the reason that the accuracy of DF systems has not improved appreciably over the last twenty years, or so, is because of the failure, on the part of system engineers, to come to grips with the effects of multipath. The objective of this project has been to study the effect of multipath on DF systems, and, in particular, the effects of multipath for different types of terrain surrounding the DF system. To achieve this goal a highly advanced eight element DF system has been developed for collecting data. This system is based on digital beamforming technology, which is increasingly finding use in advanced receiving systems. Field measurement have been carried out, and will continue to be carried out, until a statistically valid data base is established for characterizing DF propagation environments. Based on this data base, appropriate propagation models are to be developed. These will be used to develop and test DF algorithms.

One of the major activities of the current research program has been the development of a VHF measurement system for collecting multipath data. This measurement system was built by Applied Silicon Inc. Canada. Following its initial development it was used in two preliminary tests, which took place in October, 1991 and March, 1992, and the system's performance was observed to be satisfactory. A full scale field trial took place in April, 1992. However, no system no matter how well it is built is able to give perfect results. In order to enhance the accuracy of the phase measurements and to reduce the effect of aliasing, the receiving system underwent a redesign and retrofit and the new system modules are now just being completed. The upgraded system is currently undergoing system integration. A new set of measurements are expected to be recorded in the fall of 1992.

The receiving array consists of eight sensors, each consisting of a dipole antenna element. Each sensor has its own receiver. The antennas are mounted on a rotatable platform which is about five feet above the ground. In order to reduce the magnitude of diffraction (internal multipath) the antenna platform is constructed of fibre glass rather than metal. The downward force of each end of the platform is estimated to be 40 kg. Despite its size and weight it is capable of being rotated about its center. Varying signal environments, with the signals impinging from different directions with respect to the array's boresight, can be simulated by simply rotating the antenna platform. However, the task of rotating the beam takes two people, one at each end of the beam. An additional person is required to guide the other two when positioning the beam on a particular azimuth. Figures 1.1 and 1.2 give some perspective views of the platform and the antenna array.

In addition to the preliminary field trials, as described in previous interim reports, a full scale measurement trial was carried out from April 27-29, 1992. A theodolite was used for estimating the position of the signal source with respect to the array's boresight. Even though the ground was still wet at that time, the weather was warm and the mission was completed satisfactorily. The measurement trials included system calibration, single-source and two-source measurements, and measurements in the presence of artificial sources, such as metal fences, for generating an enhanced multipath environment.

In this document, we provide a description and give results, where appropriate, for the following three major activities, which were either completed or initiated during the present contract. These are as follows:

(i) the development of the multipath measurement system,

(ii) results obtained using a number of techniques for calibrating the array data, and

(iii) results obtained by analyzing some real array data.

2. PMMS SYSTEM SPECIFICATIONS

2.1 General Description

The PMMS is an 8-element VHF multipath measurement system, which consists of an eight-element antenna array. The configuration of the array is quite arbitrary. Initially, though most of the measurements will be recorded with the array configured as a linear array. Each element of the array has its own receiver, consisting of RF, IF, filter, data acquisition, and control sections. An overall block diagram of the system is given in Figure 2.1.

In the front-end modules the received signals are amplified, filtered, and downconverted to an intermediate frequency (IF) of 25 MHz. The low IF frequency provides for increased system performance in subsequent sections. Coherent detection of the signals is carried out in the final stage of the IF section. Inphase (I) and quadrature phase (Q) components of the received signals are derived by mixing each channel with reference signals that are 90 degrees out of phase with each other. One of the eight IF channel block diagrams is shown in Figure 2.2. If the received signals contain multipath components, or the signals arrive off-boresight, there will be a phase difference between the reference and received signals. This phase difference can be derived from the output of the coherent detectors. The inphase (I) and quadrature phase (Q) give the real and imaginary components of the received signals. The local oscillator (LO) and the reference oscillator are both generated from the output of a common stable source, thereby ensuring that the two oscillators are phase correlated (coherent). The frequency of the transmitted signal (beacon signal) for the initial measurements was selected to be 72.56 MHz and that of the IF to be 25 MHz. When arriving at the value for the latter frequency, Applied Silicon realized that the choice was a trade-off. The lower the value, the greater the selectivity and gain of the system. On the other hand, a low value causes the image of the received signal to be located close to the desired signal and hence decreases the signal-image ratio. This can result in undesirable mixer products appearing in the receiver channels.

2.2 System Upgrade

After discussions with Applied Silicon it was soon realized that a further system upgrade was required in order to improve both the system's efficiency and the accuracy of its measured data. It was suggested that the IF dynamic range, i.e. the minimum detectable signal that could be accurately resolved, would be improved by reducing the IF bandwidth to 200 kHz and by introducing digitally controlled 5th-order switched capacitor low-pass video filters in each of the I and Q video channels. In addition, it was suggested that a phase control adjustment be included on the front panel to adjust the phases of the 10.70 MHz reference signals. This would allow the phases of all eight

modules to be adjusted to the same zero phase position.

All of these measures were carried out. Also, an adjustment for IF gain was added so that the IF modules would all have the same gain after calibration.

It should be noted that the choice of 10.70 MHz for the IF frequency was based on the fact that standard off-the-shelf IF filters could easily be purchased. The ceramic filters that were selected have low-loss and high selectivity. Their addition to the system will have the effect of minimizing the effect of close-in interference. In addition, the phase detectors, both I and Q, are more efficient at this frequency and have better LO to RF input isolation; again, helping to improve the accuracy of the recorded data.

Fifth-order low pass video filters have been used in the outputs of the I and Q phase detectors. The design approach that was followed in the overall filter design has been to incorporate digital selection (or modification) of the video low pass corner frequency (switch selectable) so that changes in sampling rate of the A/Ds can be accommodated without a system re-design. In addition to improving system flexibility, this approach minimizes the effect of aliasing from higher frequency components in the detected I and Q signals. The long term stability of the low pass filters will be determined solely by the stability of the crystal controlled oscillator source which drives the filters. Details of the upgraded PMMS system specifications are provided in Appendix 1.

2.3 Data Acquisition

The operation of the data acquisition unit, which is shown in Figure 2.3, is rather simple and straight forward. The data collection is initiated by calling the program "DANY\EDC488" which asks the operator to enter the parameters and data identification information. The data acquisition starts and ends by hitting any key on the keyboard. The acquisition time is the period between the first hit and the second hit of any keyboard keys.

The data is stored directly onto the hard disk in binary format at the rate specified in the data collection parameters (maximum sampling rate for the 16 channels is at 1000 samples per second per channel). Once the data acquisition program is stopped, two files are created by the program: a document file (★.doc) which contains the parameters and the identification, and a data file (★.dat). These two files can then be transferred to a floppy disk for analysis on other computer systems.

The data file is partitioned in 4 kilo-byte blocks. The minimum increment for data processing is 4 kilo-bytes. A simple computer program is needed to decode the data file. The data format is as follows:

First 2 kilo-bytes:

word 1:	antenna 1	I value	sample 1
word 2:	antenna 2	I value	sample 1
:	:	:	:
:	:	:	:
word 8:	antenna 8	I value	sample 1
word 9:	antenna 1	I value	sample 2
word 10:	antenna 2	I value	sample 2
:	:	:	:
:	:	:	:
word 16:	antenna 8	I value	sample 2
word 17:	antenna 1	I value	sample 3
:	:	:	:
:	:	:	:
word 1017:	antenna 1	I value	sample 128
:	:	:	:
:	:	:	:
word 1024:	antenna 8	I value	sample 128

Second 2 kilo-bytes:

word 1025:	antenna 1	Q value	sample 1
word 1026:	antenna 2	Q value	sample 1
:	:	:	:
:	:	:	:
word 1032:	antenna 8	Q value	sample 1
word 1033:	antenna 1	Q value	sample 2
word 1034:	antenna 2	Q value	sample 2
:	:	:	:
:	:	:	:
word 1040:	antenna 8	Q value	sample 2
word 1041:	antenna 1	Q value	sample 3
:	:	:	:
:	:	:	:
word 2041:	antenna 1	Q value	sample 128
:	:	:	:
:	:	:	:
word 2048	antenna 8	Q value	sample 128

The first 4 kilo-byte block contains samples 1 to 128. The second 4 kilo-byte block contains samples 129 to 256, etc.. Each block contains 128 samples of each antenna output, in its complex form (I and Q). Each word is 16 bits long, with the high byte first (first byte is bits 8 to 15) and low byte second (second byte is bits 0 to 7). The magnitude

of a signal given by the hexa-decimal word, 7FFF, is +5 volts and that of FFFF is equivalent to -5 volts. The last data block, which is probably less than 4 kilo-bytes should not be used.

2.4 System Calibration

Prior to any measurements being recorded, system calibration must be carried out. The system parameters that are used for calibration can be recorded during the time that the off-line analysis is taking place. These parameters are then used to calibrate the amplitude and phase differences between channels that are due to the variations in the components comprising each of the channels. Differences in the signals that are due to sources of error which originate outside of the system require other techniques for calibration. The calibration procedure that has been used successfully to date for internal errors is as follows:

1. Turn off the transmitter power amplifier.
2. Disconnect the attenuators from the power amplifier.
3. Use the spare long cable going to the antennas, to connect the attenuators with the spectrum analyzer.
4. Attenuate the signal to obtain -90 dBm (which is equivalent to 63 dBm on the attenuator) at the test frequency (e.g. 72.56 MHz).
5. Disconnect the cable from the spectrum analyzer and bring it back to the antenna array.
6. Disconnect antenna 1 output from the channel 1 RF module input.
7. Connect the cable to channel 1 RF module input.
8. Start recording.
9. Change the attenuation to -60, -55, -50, and -45 dBm (which is equivalent to 33, 28, 23, and 18 dBm on the attenuator, respectively) during the recording (in approximately 5 second periods).
10. Stop recording.
11. Disconnect the cable from the RF module input.
12. Repeat steps 6 to 11 for antennas 2 to 8.
13. Perform a last data collection with all inputs open (disconnected). This will provide the absolute zero value for each channel, i.e. the dc offset values.
14. Reconnect all channels to their RF module inputs.
15. Reconnect the attenuators to the power amplifier.

It is recommended that at least one set of calibration data be recorded every time that the system is powered on. This should be carried out before data acquisition is initiated.

3. SIGNAL MODEL

Consider a uniformly-spaced linear array antenna consisting of M elements, and with N plane waves arriving at the array from distinct directions. We assume that all these plane waves are narrowband, with the same carrier frequency f_c. Figure 3.1 illustrates the configuration of a linear array with a single incident wave, denoted as n*th* wavefront, arriving from a direction defined by the angle θ_n with respect to the boresight of the array. When taking account of the gain and phase errors, the received signal at the m*th* element of the array can be described by

$$X_m = G_m \sum_{n=1}^{N} e^{j(m-1)\varphi_n} S_n + V_m, \tag{1}$$

$$\varphi_n = \frac{2\pi}{\lambda} d \sin(\theta_n) \tag{2}$$

where G_m, is a complex constant, which represents the gain and phase error at the m*th* element, S_n is the complex amplitude of the n*th* radiated signal, V_m is the additive noise, d is the interelement spacing, λ (=c/f_c) is the wavelength, and c is the wave propagation velocity. Equation (1) may be expressed in vector notation as follows:

$$X(k) = G(k) \cdot A \cdot S(k) + V(k); \qquad k = 1, 2, \cdots, K \tag{3}$$

where k is the index identifying independent data samples and

$$X(k) = [\, X_1(k), X_2(k), \cdots, X_M(k) \,]^T, \tag{4}$$

$$S(k) = [\, S_1(k), S_2(k), \cdots, S_N(k) \,]^T, \tag{5}$$

$$V(k) = [\, V_1(k), V_2(k), \cdots, V_M(k) \,]^T, \tag{6}$$

$$G = diag\{ \alpha_1 e^{-j2\pi f_c \tau_1}, \alpha_2 e^{-j2\pi f_c \tau_2}, \cdots, \alpha_M e^{-j2\pi f_c \tau_M} \}, \tag{7}$$

$$A = [\, a(\theta_1), a(\theta_2), \cdots, a(\theta_N) \,], \tag{8}$$

$$a(\theta_n) = [1, e^{-j\varphi_n}, \cdots, e^{-j(M-1)\varphi_n}]^T, \tag{9}$$

in which $(\cdot)^T$ represents the transpose operation, $a(\theta_n)$ is a steering vector of the n*th* signal, S(k) is a signal vector with covariance matrix $\sigma_s^2 \cdot I$, and V(k) is a noise vector with zero mean and covariance matrix $\sigma_n^2 \cdot I$, where I is an identity matrix.

For our simulation studies, the gain of the sensors was selected using the following relation:

$$\alpha_m = [(\xi_m - 0.5)\sigma_\alpha \cdot \sqrt{12} + 1]; \qquad m = 1, 2, \cdots, M \tag{10}$$

where ξ_m is a uniformly distributed random number between zero and one and σ_α^2 is the variance of the gain. The phase of each of the sensors was selected according to

$$\Psi_m = [(\gamma_m - 0.5)\sigma_\psi \cdot \sqrt{12}]; \qquad m = 1, 2, \cdots, M \tag{11}$$

where γ_m is a uniformly distributed random number between zero and one and σ_ψ^2 is the variance of the sensors phase. The element signal to noise ratio SNR is defined as

$$SNR = 10 \log_{10}\left(\frac{\sigma_s^2}{\sigma_n^2}\right). \tag{12}$$

The calibration techniques that are introduced in the next chapter for estimating gain and phase errors of the array signals are based on eigen-decomposition of a sample covariance matrix, derived from the vector of received signals. It should be noted that the gain and phase errors being referred to here consist in part of those that remain after the internal calibration procedure has been applied to the measurement system. They go beyond the residue of the internal calibration and include errors caused by external sources, such as mutual coupling between the antenna elements, misalignment of the antenna elements, changes in electrical lengths of coaxial cables due to temperature changes, scattering from topological features located near the antenna array, etc. Basically, most of these errors are due to complexities in the instrumentation and environment which cannot be included in the signal model. Therefore, they must be treated as errors rather than deterministic phenomenon. Since the calibration techniques are based on eigen-decomposition, they are bounded by the same assumptions that apply to the MUSIC algorithm and other eigen-structure based methods used for direction finding. Standard assumptions are stated as follows:

(1) The signals and the noise processes are stationary and ergodic over the observation period.
(2) The columns of B = G · A are linearly independent.
(3) The signals are not perfectly correlated.
(4) The noise is uncorrelated with the signals and its covariance matrix is full rank and is known except for a multiplication constant σ_n^2.

The covariance matrices of the signal, noise, and observation vectors are given by

$$R_s = E\{SS^H\}, \tag{13}$$

$$\sigma_n^2 \cdot I = E\{VV^H\}, \tag{14}$$

$$R_x = E\{XX^H\} = GAR_sA^HG^H + \sigma_n^2, \tag{15}$$

where E{·} denotes the expectation of the bracketed parameter and $(\cdot)^H$ represents the Hermitian transpose operation. Let λ_i and $\mathbf{u}_i$, i=1,2,···,M be the eigenvalues and corresponding eigenvectors of the covariance matrix R_x, (i.e., the solutions of $R_x\mathbf{u} = \lambda\mathbf{u}$), where the λ_i are listed in descending order. Each of the columns of B = G·A is orthogonal to the matrix $U=[\mathbf{u}_{N+1}, \mathbf{u}_{N+2}, \cdots, \mathbf{u}_M]$.

With the inclusion of the error matrix G in the expression B=G·A, the eigenvalues λ_i are implicitly composed of two components: the signal and the calibration errors due to gain imbalance in the array elements, and so as well the corresponding eigenvectors $\mathbf{u}_i$. If the first N eigenvalues of the matrix R_x are large enough to determine the number of signal sources, N, then the first N eigenvectors and the last M-N eigenvectors can be used as the estimates of the signal subspace and the noise subspace of the array covariance matrix. Since the signal subspace and the noise subspace are assumed to be uncorrelated, they are orthogonal subspaces. If U is truly an exact representation of the noise subspace, it implies

$$U^H a(\theta_n) = 0 \tag{16}$$

where 0 is a null vector. Unfortunately, due to the presence of gain and phase errors in array elements, U is corrupted and the equality in Equation (16) does not usually hold. In fact, the noise subspace U is orthogonal to the vector $\mathbf{a}(\hat{\theta}_n)$, where $\hat{\theta}_n$ is an estimate of the true angle of arrival θ_n, where

$$a(\hat{\theta}_n) = G\,a(\theta_n) \tag{17}$$

with G an MxM diagonal matrix. Equation (16) becomes

$$c_n = U^H G\,a(\theta_n) = 0\,. \tag{18}$$

It follows that an antenna system will be precisely calibrated if the diagonal error matrix G is known in advance.

4. CALIBRATION TECHNIQUES

The presence of gain and phase errors in the signals obtained from a DF array will usually lead to a critical deterioration in the performance of the DF system, in terms of its accuracy and ability to resolve the DOA of closely spaced incoming signals. In fact, this is known to be one of the major problems standing in the way of the implementation of superresolution with practical DF systems. Once a truly accurate means of calibration is derived then simple superresolution techniques can be used for achieving a considerably improvement in the accuracy of DF systems. Three calibration techniques are investigated in this study. To measure the success of each of these techniques, a data set is corrected using each of the techniques -each of the corrected data sets is then used to derive the DOA of the array signals and/or to reconstruct the beam pattern of the receiving array. As a measure of the success of each technique, the result obtained from each of the corrected data sets is compared with ground-truth data. The techniques are the following: (i) Ho's array calibration algorithm [1], (ii) Friedlander and Weiss's self calibration algorithm [2], and (iii) calibration by experimental data.

4.1 Ho's Array Calibration Algorithm

The calibration method developed by Ho [1] is an iterative method. It is based on the eigen-based structure method. Optimal DOAs are estimated via the least-squares norm minimization. By expanding Equation (18) a system of linear equations is obtained as

$$c = \begin{pmatrix} c_1 \\ c_2 \\ \cdot \\ \cdot \\ \cdot \\ c_N \end{pmatrix} = \begin{pmatrix} UGa(\theta_1) \\ UGa(\theta_2) \\ \cdot \\ \cdot \\ \cdot \\ UGa(\theta_N) \end{pmatrix}, \tag{19}$$

and is defined as a calibration vector where c is a N(M-N)x1 vector. By utilizing the equivalent notation

$$G\,a(\theta_n) = Q(a(\theta_n)) \cdot \delta \tag{20}$$

where $Q(a(\theta_n))$ is a MxM diagonal matrix whose elements are those of steering vector

$a(\theta_n)$, and δ is a vector of the array error, i.e.,

$$\delta = [G_{11}, G_{22}, \cdots, G_{MM}]^T, \tag{21}$$

$$Q(\theta_n) = diag\{a(\theta_n)\}. \tag{22}$$

Rewrite Equation (19) as

$$c = T\delta \tag{23}$$

where

$$T = \begin{pmatrix} T_1 \\ T_2 \\ \cdot \\ \cdot \\ \cdot \\ T_N \end{pmatrix} = \begin{pmatrix} U\,Q(\theta_1) \\ U\,Q(\theta_2) \\ \cdot \\ \cdot \\ \cdot \\ U\,Q(\theta_N) \end{pmatrix}. \tag{24}$$

The matrix T in Equation (24) of dimension N(M-N)xM is defined as the projection calibration matrix. By applying singular value decomposition, the matrix T is decomposed into the form

$$T = U_L \Lambda U_R^H \tag{25}$$

where U_L is a N(M-N)xN(M-N) column matrix of the left singular vectors, U_R is a MxM column matrix of the right singular vectors and Λ is a diagonal matrix of the singular values β_m, in which

$$\beta_1 \geq \beta_2 \geq \cdots \geq \beta_{M-1} \geq \beta_M. \tag{26}$$

In the error free case the vector δ in Equation (21) is a unique vector and the calibration vector c becomes a null vector. In this case, the matrix T must be a singular matrix of rank M-1 (i.e. its M*th* singular value β_M=0). Similarly, for the case of gain and phase errors in array signals, if it is assumed that K(M-K)≥M, and if further it is assumed that the rank of the matrix T is M-1, then the right singular vector U_{RM} of the

matrix T is the least-squares norm estimate [5] of the error vector δ. As well, under these assumptions, the angles θ_ns, which are used to form the matrices Q, are the minimum norm least-squares estimates of the DOAs.

The algorithm for minimizing the residual norm may be described as follows:

(1) Set the iteration counter to zero, e.g., i=0.

(2) Initialize the gain-phase matrix G = I, an identity matrix.

(3) Form the array covariance matrix as defined by

$$R_x = \frac{1}{K}\sum_{k=1}^{K} X(k)\,X(k)^H. \tag{27}$$

(4) Estimate the noise subspace U.

(5) Assume one of the signal location is known, e.g. $\theta_1 = \theta_{reference}$.

(6) Use the subspace method (MUSIC), as given in Equation (28), to search for the N highest peaks of the spatial spectrum and to estimate the DOAs, i.e., θ_ns.

$$P^{(i)}(\theta) = \| U^H G^{(i)} a(\theta) \|^{-2}. \tag{28}$$

(7) For each set of $\hat{\theta}_n$s, the estimated DOAs, obtain the projection covariance matrix T.

(8) Compute the least-square norm

$$\mu(\hat{\theta}_i s) = \| c \|^2 = \| T U_{RM} \|^2 \tag{29}$$

where i denotes the number of iterations, and U_{RM} is the M*th* column of the right singular vector of matrix T decomposed using the SVD.

(9) Repeat steps (6) to (8) for all $\hat{\theta}_n$s. The set of $\hat{\theta}_n$s at which $\|c\|^2$ is minimum will correspond to the optimal estimate of the DOAs.

Simulation results using Ho's calibration method are shown in Figure 4.1 and Figure 4.2. An eight element array with interelement spacing d=λ/2 was used for the simulations. The variance of the gain and phase errors were 0.5 and 20°, respectively.

The SNR for the simulated data in Figure 4.1 was 30dB and that for Figure 4.2 was 20dB. The DOA estimates in Figure 4.1a are -10° and 4.8°. These were obtained after six iterations and are in excellent agreement with the true DOA, specified at -10° and 5°. Additionally, the DOA estimates in Figure 4.2a converged to -5° and 3.4° after fifteen iterations. They are exceptionally close to the defined DOAs, -5° and 3°. Figures 4.1c, 4.1d, 4.2c, and 4.2d demonstrate how the estimated gain and phase of the antenna elements converges to its actual value during some iteration stages. A unity gain and zero phase represented the initialization for the first iteration. Both results displayed good convergence characteristics as shown in Figures 4.1b and 4.2b. However, a theoretical proof for the convergence of the least-square norm has not yet been provided by Ho.

4.2 Friedlander - Weiss's Self Calibration Algorithm

Friedlander and Weiss's method is based on the eigendecomposition of the sample covariance matrix of the vector of received signals. In addition to the standard assumptions underlying the MUSIC algorithm there is a necessary condition that needs to be satisfied in order to guarantee the existence of a solution. Referring to the basic Equation (15) where R_x can be perfectly described by $2MN - N^2 + 1$ parameters. These parameters are the N + 1 different (real) eigenvalues and $2NM - N^2 - N$ parameters that define the N complex eigenvectors describing the signal subspace, that satisfy N(N+1)/2 complex orthogonality constraints. On the other hand, there are $r \cdot N$ unknown location parameters (r=1 for azimuth only system, r=2 for azimuth and elevation system, etc.) - N^2 unknown parameters that define the Hermitian matrix R_s, a single unknown parameter σ_n^2, and 2(M-1) parameter associated with G. Thus, a solution may exist if

$$2MN - N^2 + 1 \geq r \cdot N + N^2 + 1 + 2(M-1), \tag{30}$$

$$M \geq \frac{2N^2 + r \cdot N - 2}{2(N-1)}. \tag{31}$$

It is suggested that one should first estimate R_x and use the estimates of the eigenvectors to estimate the number of signals. Once N is known reasonable estimates of $\{\theta_n\}$ and G may be obtained by minimizing the cost function

$$J_c = \sum_{n=1}^{N} \| U^H \hat{G}\, a(\theta) \|^2 \tag{32}$$

which is the squared Euclidean norm of the matrix $U^H \hat{G} a(\theta)$.

The minimization algorithm is based on two main procedures. First, the gain-phase is assumed (approximately) to be known, and $\{\theta_n, n=1,\cdots,N\}$ may be estimated using the basic principles underlying the MUSIC algorithm. Given estimates of $\{\theta_n\}$, J_c may be minimized over the gain-phase parameters. This minimization procedure can be repeated until J_c converges. The algorithm for minimizing the cost function may be described as follows:

(1) Set the iteration counter i to zero.

(2) Select initial values for the gain-phase matrix G. Usually the initial values are based on some previous knowledge or predictions based on an idealized model.

(3) Use all available data vectors to compute the data covariance matrix as in Equation (27).

(4) Perform eigen-analysis and construct U.

(5) Search for the N highest peaks of the spatial spectrum defined by Equation (28). These peaks are associated with the N DOA's $\{\theta_n, n=1,\cdots,N\}$. Also note that substituting the $\{\hat{\theta}_n^{(i)}\}$, so estimated, in J_c guarantees that $J_c^{(i)}$ is minimized for given $G^{(i)}$.

(6) Fix the DOAs and minimize the cost function J_c with respect to the gain and phase of each of the sensors. J_c becomes

$$J_c = \sum_{n=1}^{N} a(\theta_n)^H \hat{G}^H U U^H \hat{G}\, a(\theta_n). \tag{33}$$

(7) Utilizing the equivalent notation in Equation (20), J_c may be rewritten as

$$J_c = \underline{\delta}^H \{\sum_{n=1}^{N} Q^H U U^H Q\} \underline{\delta}. \tag{34}$$

(8) Minimize Equation (34) with respect to $\underline{\delta}$ under the constraint $\underline{\delta}^H \mathbf{w}=1$, where $\mathbf{w} = [1,0,0,\cdots,0]^T$. The result of this quadratic minimization problem under linear constraints is well known and given by

$$\hat{\underline{\delta}} = \frac{Z_i^{-1} w}{w^T Z_i^{-1} w} \tag{35}$$

where Z_i is the matrix

$$Z_i = \sum_{n=1}^{N} Q^H U U^H Q. \tag{36}$$

(9) Compute the gain-phase matrix $\hat{G}$ from the vector δ given by

$$\hat{G}^{i+1} = diag(\delta). \tag{37}$$

The cost function J_c is thus minimized by holding the DOAs fixed and searching over the space of the sensor gain-phase parameters.

(10) Compute J_c^{i+1} using the estimated DOAs and sensor gain-phase. If

$$J_c^i - J_c^{i+1} > \varepsilon, \qquad (a\ preset\ threshold) \tag{38}$$

then update the iteration counter i=i+1 and go back to step (5). The algorithm performs the iterations until J_c converges and stops when

$$J_c^i - J_c^{i+1} \le \varepsilon. \tag{39}$$

Simulation results are given in Figures 4.3 and 4.4, based on an eight element array and an element spacing of $\lambda/2$. Both figures used the same set of DOAs, namely -30°, -5°, and 35°. It took four iterations to complete the calibration process shown in Figure 4.3a with a SNR of 20 dB, and a variance in the gain and phase of 0.2 and 20°, respectively. The estimated DOA were found to be -29.8°, -4.9°, and 35.2° after the 4*th* iteration. For a larger variance, namely 0.5 and 40° for the gain and phase errors, respectively, a longer iterative process is required as illustrated in Figure 4.4a. It is noted that the DOAs were -29.7°, -3.6°, and 32.8° after the first iteration. At the end of the 6*th* iteration, the calibrated DOAs became -30.1°, -5.1°, and 34.9°. It is clear that major DOA errors were corrected using this technique. Figure 4.3c, 4.3d, 4.4c, and 4.4d demonstrate the development in the gain and phase uncertainty associated with the antennas after each iteration. Based on these results there is no doubt that the estimated gain and phase values for each antenna converges to its actual value. Despite the lack of a proof to support the calibration algorithm, a good convergence of the cost function was observed as is shown in Figure 4.3b and 4.4b.

It is noted that the algorithm is fairly insensitive to the initial gain and phase error values. The convergence speed of Friedlander and Weiss's algorithm is faster than the one developed by Ho. The technique can be extended to include mutual coupling

between antennas and is currently under investigation.

4.3 Calibration Based on Experimental Reference Data

This technique does not require the knowledge of any array manifold, nor gain and phase channel characteristics. It is based on using a single source in a known location. A set of sampled data are then recorded and used subsequently as reference data. Any other data corresponding to signals with unknown DOAs may be calibrated using this reference data. The calibration algorithm may be described as follows:

(1) Collect measurement data with a source located at a known position.

(2) Calculate the synthetic pattern due to plane wave propagation with respect to the known DOA in (1).

(3) Normalize the generated synthetic data by the measured data in (1) to determine the gain-phase difference.

(4) Determine the calibration factor by estimating the mean of the gain-phase difference.

(5) Multiply any measured data from a source whose position is unknown by the calibration factor to obtain a set of calibrated data.

This is a very simple and straight forward calibration algorithm. It lumps all error components into a calibration factor, a vector of gain and phase values for each sensor. Despite the fact that the calibration technique may be capable of providing reasonably accurate angle of arrival estimates, the beam pattern is not as good as if the system characteristics were known and the inaccuracies were compensated. However, the method serves as a very good tool for making a first pass estimate of the performance of the receiving system without undergoing the system calibration procedures described in chapter 2. The effectiveness of this method will be demonstrated in the following section.

5. DATA ANALYSIS

Prior to the measurements, a site survey was conducted using a theodolite to define the bearing of the source position. Each defined spot was indicated by a stick and marked by an x as shown in Figure 5.1. According to the figure, the bearings measured to the right of the boresight of the array were denoted by R and a number and those to the left were represented by L. As a supplement, another site survey, as shown in Figure 5.2 was carried out using a measuring tape. It was found that both investigations gave very good agreement on the bearing estimates. Due to a technical problem with one of the receiving units, only the first seven antennas were used for recording data. Channel eight was not used for these measurements.

5.1 System Calibration

Since the electronic components of the PMMS are likely to be sensitive to temperature, humidity, and in general, environmental factors, it was realized that the gain and phase characteristics of the system's channels may change as its environment changes. Therefore, in order to ensure that the recorded data was of the highest quality, it was decided that the system be calibrated at appropriate intervals of time, and, in particular, whenever the system was powered on. The procedures listed in Chapter 2 were used for carrying out the system calibration. Also, it was thought that a comparison of the calibration data might be useful for identifying any inconsistencies or instabilities in the receiving system.

As part of the regular calibration procedure, the synthesizer and the channel under consideration were connected using the coaxial cable and the power into the system varied by varying the settings of the attenuator. The first test that was applied to see how well the system was performing was to inspect that data and see if the output and input to the system varied in a linear fashion. Calibration data were recorded on April 28 (am), April 28 (pm), and April 29, 1992 and the results are presented in Figures 5.3 to 5.5, respectively. In parts (a) and (b) of Figures 5.3 to 5.5 are given the gain and phase characteristics of the channels. Among those data, the set of data collected on April 28 (pm) reflects a better system performance than the other two sets. Linearity in the transfer characteristics was found for all seven channels. The gain and phase difference of the channels are estimated by averaging the collected data and using the results as coefficients for data calibration. The origin or the dc offset values of the channels are shown in parts (c) and (d) of Figures 5.3 to 5.5. It was found that channel 2 had an enormously high dc value which caused channel saturation in some of the measurements. Applied Silicon Inc. Canada has been so advised and the problem is under investigation.

5.2 Single Source Measurements

Data was measured using a single source at almost all locations except L4 because the distance exceeded the length of the electrical cable. Measurements were carried out at various attenuation levels. The beam patterns based on the measurements were obtained by applying a discrete Fourier transform to the collected data. Figures 5.6 to 5.12 represent the beam patterns for source locations -13.6°, -9.2°, -4.6°, 4.6°, 9.2°, 13.75°, and 18°, respectively. The figures consist of (i) a synthetic pattern generated by a plane wave at a defined incident angle, (ii) an error corrected pattern calibrated by a reference pattern which was measured with its source positioned on the boresight of the array, and (iii) a pattern based on uncalibrated data. Results documented in part (a) of the figures were based on the assumption that no prior knowledge was available for the system characteristics. On the other hand, data compensated by the gain and phase imbalance between channels were analysed and recorded in part (b) of the figures. The gain and phase imbalance between channels due to tolerance in RF components, dc offset, and unevenly cut cables were corrected by using the calibration data obtained on April 28 (pm), 1992.

It is clear when looking at these results that excellent results were realized in terms of the close agreement shown between the boresights of the derived antenna beam patterns and the known signal directions. That is, for the single source data, the estimates of DOA, based on the positions of the boresights of the main antenna beams would be very good. On comparing results given in sections (a) and (b) of these figures, it is seen that if the gain imbalances of the channels are known, then the derived beam patterns agree much more closely with the simulated patterns. Therefore, it is concluded from the single source measurements that the DOA estimates are not greatly affected by gain imbalances. (This conclusion will not hold for multiple sources, in particular, if the sources are grouped closely together.) On the other hand, it is observed that gain imbalances can greatly affect the sidelobe level and the shape of the mainbeam patterns. It was found that the shape of the mainbeam pattern was relatively invariant to changes in the signal level. These results are not included in this report. DOA estimates, based on Friedlander and Weiss's calibration method, were also derived and the results are given in Figure 5.13. It is seen that there is good agreement between the DOA predictions obtained using the Friedlander - Weiss method and the Fourier transform method.

5.3 Two Sources Measurements

Two source measurements were carried out in order to more critically examine the performance of the PMMS system, and also, to study various beamforming techniques. Two types of measurements were carried out; namely, coherent source measurements and incoherent source measurements.

For the coherent source measurements, a second transmitting antenna was brought in and the signal to this antenna was derived from the source used with the original antenna. In so far as there are no system instabilities, this arrangement insures that the two signals are truly coherent. The two transmitted waveforms differ only by a constant phase and a constant difference in their power levels. Measurements were carried out using azimuthal separations of 9.2° and 13.6°. Figures 5.14 and 5.15 show the beam patterns that were obtained by applying Fourier transforms to the recorded data. When the azimuthal separation of the two sources was less than a beamwidth, a broadened beam pattern was observed as shown in Figure 5.14. As the separation of the sources was increased, two peaks started to emerge. The peaks became truly distinct when the separation was equal to a beamwidth. However, in Figure 5.15, where the peaks are indeed distinct, we see that their azimuths are -16.33° and 3.13°, somewhat removed from the true azimuths, i.e. -13.6° and 0°. This discrepancy is thought to be due to the fact that for this result the source separation is somewhat less than the 3 dB beamwidth of the antenna. For a seven element array this is calculated to be 16.8°.

Most high-resolution direction finding techniques are based on the assumption that the sources are uncorrelated. Since in practice this is often the case, it is desirable to obtain data using uncorrelated sources. Measurements were carried out using two incoherent sources. Unfortunately, some technical problems were experienced during the measurements and the data turned out not to be of high quality. It was found that the power radiated by the second source was frequency dependent and as a result its level was considerably higher than that of the original transmitter. This resulted in some of the channels becoming saturated - this was particularly true of channel 2. Another set of trials will be carried out in the near future. It is expected that we will easily achieve our objective of recording and analyzing incoherent source data.

5.4 Measurements in the Proximity of a Fence

When a target lies in close proximity to a reflecting surface (e.g. ground, sea surface, buildings, etc.), the received signal may reach the antenna via a multiplicity of paths (i.e. two or more), even though only one source may exist in reality. By the same token multiple paths may be generated by objects in the vicinity of a DF system if they reflect some portion of the signal from the source in the direction of the DF system. This is called the multipath phenomena. It results in a multiplicity of sources, where in fact only one true source exists. Overcoming the degradation in the performance of DF systems, due to multipath, is the main issue that is being dealt with in this study.

A poultry fence whose length was about 6.45m and height was 1.8m was used as a source of multipath signals. Its configuration relative to that of the PMMS is shown in Figure 5.2. Measurements were carried out using one source. Data were collected with the source located at -4.6° and 9.2° with respect to the boresight of the receiving array. The beam patterns corresponding to the source positions of -4.6° and 9.2° are given in

Figures 5.16 and 5.17, respectively. The figures contain (i) a synthetic pattern generated by a plane wave at a specified incident angle, (ii) a calibrated pattern without the presence of fence, and (iii) a calibrated pattern with the presence of fence. In Figure 5.16, no change in the main lobe of the beam pattern can be found for the source located at -4.6°. However, there is a drift in the beam pattern for the source at 9.2°, as indicated in Figure 5.17.

At first, it was thought that the shift may be due to multipath generated by the poultry fence. Unfortunately, the drift direction was somewhat contradicted by our predicted result. Through observation, analysis may be outlined as follows:

(1) If a multipath signal exist, the position of the main beam should drift in the direction of the multipath source with respect to the array.

(2) If the beam is a resultant of the direct and indirect sources, a broadened beamwidth should occur.

According to Figure 5.17, it is clear that both conditions (1) and (2) are not satisfied. The shifted pattern, perhaps is not due to the fence. However, there is a possibility that the shift in pattern may still be caused by the fence but under the effect of glint [6].

As described in [6], glint is defined as the inherent random component of error in measurement of position or doppler frequency of a complex target due to interference of the reflections from different elements of the target. In the case of two element target the glint error with respect to the center point of the target pair is given by

$$\chi = \left(\frac{1}{2}\right) \frac{1 - k^2}{1 + k^2 + 2k\cos(\gamma)} \qquad (40)$$

where k is the ratio of amplitude of target 2 to target 1 and γ is the relative phase angle between the two signal components. This is plotted in Figure 5.18 as a function of phase angle γ for different values of k. It is important to note that the magnitude of the glint error depends on k and γ while the direction of the glint deviation is a function of k. For small k, the deviation in the tracking of target will oscillate sinusoidally about the position of the stronger source.

In our multipath measurement the specular multipath component due to reflection from the fence can be assumed as a second target and the value of k is often less than 1. If the DOA of the source and the arrival angle of the multipath component cannot be resolved, the resultant beam will then oscillate sinusoidally about the source. According to the site survey in Figure 5.2 with the source at R2 and the measurement set-up for Figure 5.17, the phase difference between the direct signal and the multipath signal based on their path difference and the phase change (π) upon reflection was calculated

unless k, the ratio of the amplitude of multipath component to the source is known. It is believed that the theory of glint may explain the result in Figure 5.17. Nevertheless, this remains to be verified by the next set of measurement.

The effect of glint can simply be illustrated by carrying out a measurement using two correlated sources. The value of k may be measured by using a power meter. However, no conclusions will be drawn at this point until a re-measurement is conducted with the upgraded system.

6. CONCLUSIONS AND FUTURE WORK

Gain and phase errors that occur in the signals appearing at the outputs of the elements of antenna arrays create practical problems for DF systems. It is believed that any high-resolution DF algorithm, exhibiting the most outstanding characteristics in terms of the accuracy of its estimates, can be implemented in a DF system if an appropriate calibration coefficients can be derived and then applied to elements of the antenna array. By appropriate is meant; with "the required level of accuracy". Three calibration techniques were studied in this report. The first was an array calibration algorithm that was developed by Ho. This technique requires some a priori information; namely, that the DOA of one of the signal's used for calibrating the array be known. If this condition is satisfied, the DOA of the other signal being used in the calibration is derived during the calibration procedure, as well as the calibration coefficients. It was found that in Ho's method the minimization of the least-squares norm, based on singular decomposition, gives a good estimate of the unknown DOA. Sometimes Ho's techniques was seen to exhibit a slow rate of convergence. The second self calibration technique, that developed by Friedlander and Weiss, gives a good estimate of DOAs and was observed to converge faster than Ho's method. Moreover, the technique can be extended to include mutual coupling between the elements of the antenna array. The last calibration technique that was investigated was based on recording a data vector using a source whose DOA was known a priori. The recorded data vector was used to derive a vector of calibration coefficients. The calibration coefficients were used to calibrate the data for signals with unknown DOAs. It was shown that in the case of a single source that after calibration of the data vector corresponding to a signal with an unknown DOA, the DOA estimates were very accurate. It was observed that despite the fact that the DOA estimates were reasonably accurate, the beam patterns derived from the calibrated data vectors showed significant distortions and high sidelobe levels.

This simple calibration technique has not yet been tested for the case of two unknown signals. Of particular interest would be the case where the signals were separated by less than a beamwidth. As well, it could turn out to be a most useful exercise if the calibration measurements were to be carried out for all signal DOAs, and then, based on these measurements, a catalogue of calibration coefficients was derived and stored in computer memory. This, of course, would be easily accomplished using the PMMS system because the antenna array is mounted on a rotatable platform. In practice, measured values of unknown signal DOA would be refined by choosing the appropriate calibration coefficients and applying them to the initial data vector. As a first pass, the initial data vector would be Fourier transformed to derive a course value for the DOA. This quantity would then be refined by choosing the calibration coefficients that correspond to the approximate DOA, applying the coefficients to the initial data vector and then applying either a Fourier transform or a superresolution algorithm to the corrected data vector.

Despite some unexpected delays due to a number of factors, measurements were carried out using the VHF multipath measurement system and satisfactory results were obtained. The successful measurements consisted of; (i) system calibrations, (ii) single source measurements, and (iii) coherent source measurements. Perhaps it comes as no surprise, that the single source DOA estimates proved to be robust and showed very good accuracy. As well, the signal source beam patterns were seen to be reasonably close replicas of the simulated patterns. Unfortunately, it was observed that the channel characteristics of the system were found to exhibit some instabilities. It is believed that the upgraded system will provide better DOA estimates and will exhibit a more stable performance than the present system. It turned out to be somewhat disappointing that the incoherent source measurements could not be analyzed due to channel saturation. Otherwise, a more thorough study could have been carried out deriving calibration vectors, based on the techniques described in this report, and applying them to the measured data vectors. It is also believed that multipath component may create a deviation in the DOA estimates under the phenomena of glint effect. More measurements will be carried out in order to verify the effect of glint.

A considerably large measurement program is required in order to build a sufficiently large data base so that multipath characteristics subject to different vegetation backgrounds are accurate reflections of the real environment. Upon completion of the upgraded system, more measurements will be carried out which will include, but not necessarily be restricted to,

(1) Data sampling under different vegetations and terrains.

(2) Measurements using incoherent source.

(3) Experiments using stationary and mobile multipath sources.

(4) Generation of two-dimensional interference patterns.

(5) Illustration of the glint effect using two sources.

(6) Generation of comprehensive calibration data bases.

On the other hand, a comprehensive analysis of the measured data will be carried out which will include, but not necessarily be restricted to,

(1) Calibrating the data using all three calibration techniques as studied in this project.

(2) Applying temporal autocorrelation to the data obtained from the individual elements.

(3) Applying spatial cross-correlation to the data obtained from the complete array aperture.

(4) Using FFT based direction finding techniques to localize major multipath components.

(5) Applying superresolution direction finding techniques, such as the maximum likelihood method, to resolve fine-scale multipath components.

(6) Determining DF errors for various types of terrain, as well as different kinds of DF algorithm.

(7) Developing a signal-noise model for unresolvable multipath signals.

P148381.PDF [Page: 44 of 87]

References

[1] Ho, T.V.: 'Novel techniques and architectures for adaptive beamforming', Ph.D. Thesis, Department of Electrical and Computer Engineering, McMaster University, 1990.

[2] Friedlander, B. and Weiss A.J.: 'Direction finding in the presence of mutual coupling', *IEEE Trans. Antennas and Propagation*, Vol. 39, No. 3, pp. 273-284, March 1991.

[3] Haykin, S.: *Array Signal Processing*, (Edited by S. Haykin), Prentice-Hall, Inc., 1985.

[4] Goldman, S.J.: *Phase Noise Analysis in Radar Systems Using Personal Computers*, John Wiley Sons, 1989.

[5] Pualraj, A. et al.: 'A subspace approach to determining sensor gain and phase with applications to array processing", *Proc. SPIE*, Vol. 696, pp. 102-107, 1986.

[6] Barton, D.K.: Modern Radar System Analysis, Artech House, Inc., 1988.

APPENDIX 1

UPGRADED PMMS SYSTEM SPECIFICATIONS

RECEIVER RF SECTION

RF input noise figure	6.0 dB maximum
RF to IF conversion gain	12 dB
RF input frequency range	25 MHz to 80 MHz
LO input frequency range	95 MHz to 25 MHz
LO input signal	-12 dBm nominal
IF output centre frequency	10.70 MHz
IF output bandwidth	2 MHz
RF dynamic range	85 dB (linear range)
Minimum RF input	-112 dBm
Maximum RF input	-30 dBm (system saturation)
Absolute maximum RF input	+5 dBm (without damage)

RECEIVER IF SECTION

IF centre frequency	10.70 MHz
IF bandwidth	200 KHz nominal
IF gain	70 dB nominal
IF dynamic range	40 dB (note 1)
Full IF dynamic range	85 dB
Digital IF gain control range	42.0 dB in 1.0 dB steps
Manual IF gain control range	10.0 dB
Output	I & Q phase single ended
I & Q video bandwidth	selectable 6 bandwidth from 10 Hz to 300 Hz
Phase balance	±4 degrees (note 2)
Amplitude balance	±.1 dB or 3 mV, whichever is greater (note 2)

Note 1: The IF dynamic range is without any switched IF attenuation.

Note 2: Phase balance and Amplitude balance are relative to the IF module input only.

OSCILLATOR MODULE

Primary output frequency	2 MHz to 100 MHz
Primary frequency step size	5.0 KHz
Primary frequency control	manually set switches
Reference frequency	10.70 MHz
Reference frequency control	internal switches
Reference frequency step size	5.0 KHz
Frequency reference	324 MHz crystal oscillator

POWER SUPPLY MODULE

Primary input power	110 Vac ± 10%
Power capacity	120 watts
Output voltage	+15 Vdc, -15 Vdc, and -6 Vdc

A/D CONVERTER

A/D sampling rate	1000 samples/sec maximum
A/D resolution	16 bits
A/D effective accuracy	12 bits
Aperture uncertainty	40 ns

TRANSMITTER MODULE

Output frequency	2 MHz to 100 MHz
Frequency step size	5.0 KHz
Primary frequency control	manually set switches
Frequency reference	324 MHz crystal oscillator
Maximum TX output power	3.0 watts
TX power output control	manually set switches
Primary input power	110 Vac ± 10%

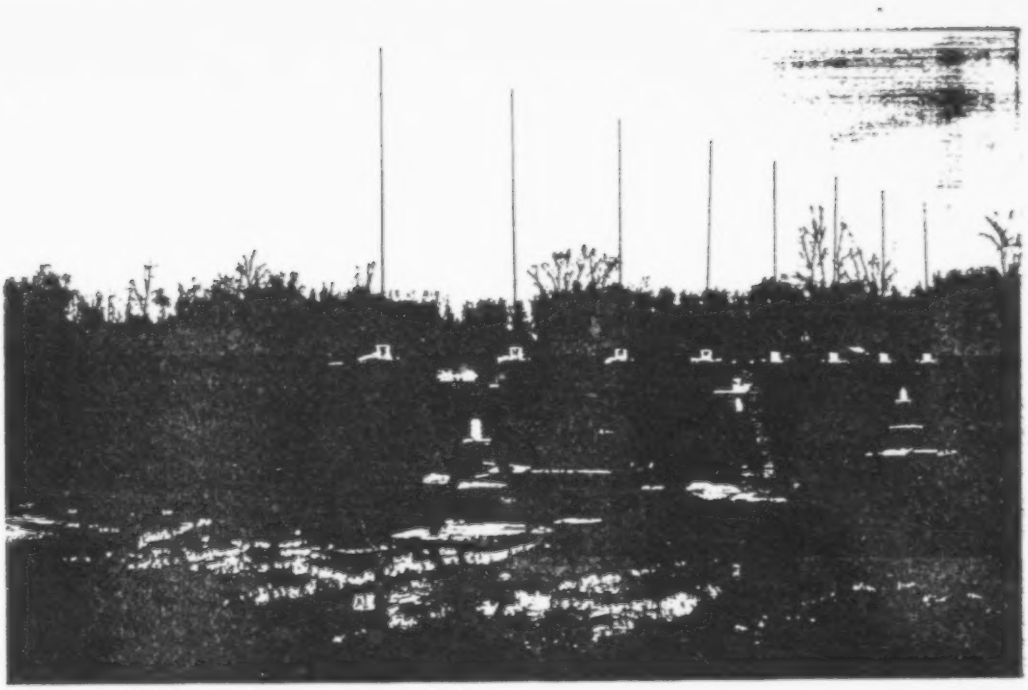

Figure 1.1 A linear array rests on a fibreglass platform.

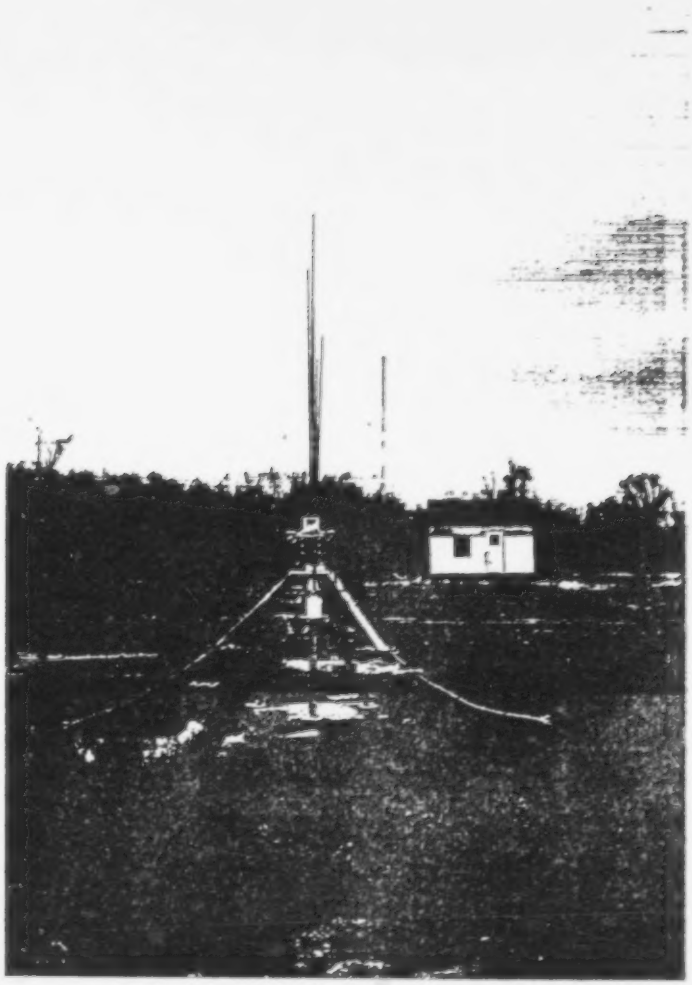

Figure 1.2 Another view of the linear array and its platform.

P148381.PDF [Page: 51 of 87]

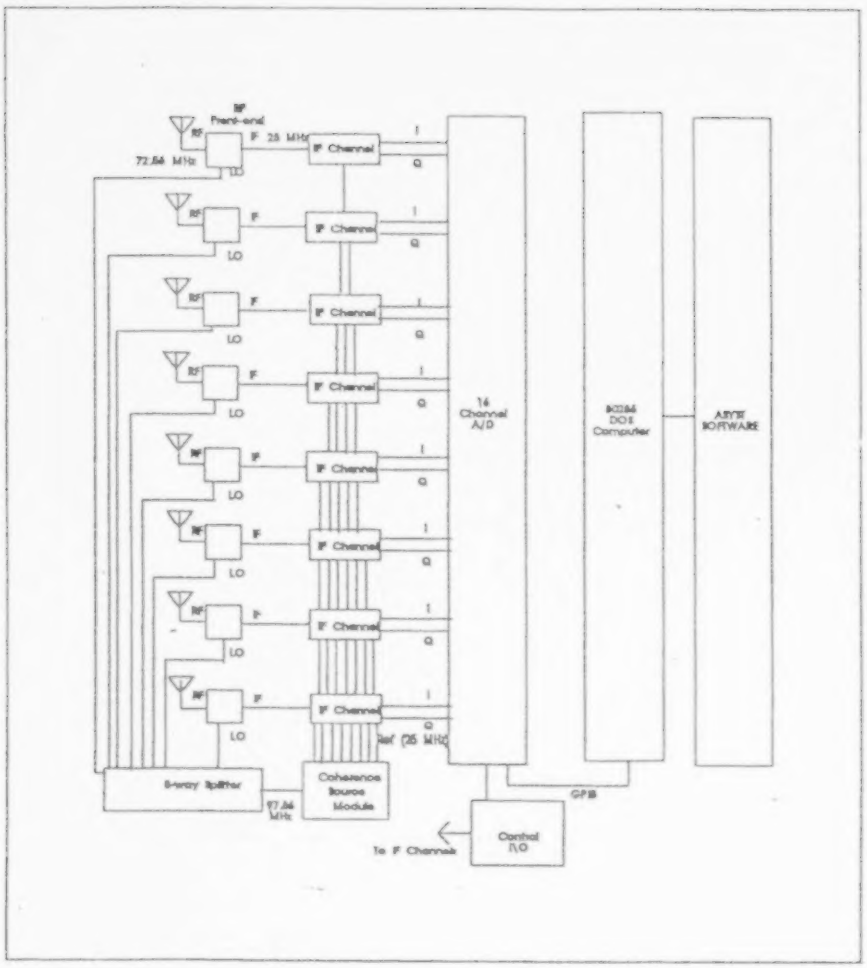

Figure 2.1 A block diagram of the multipath measurement system.

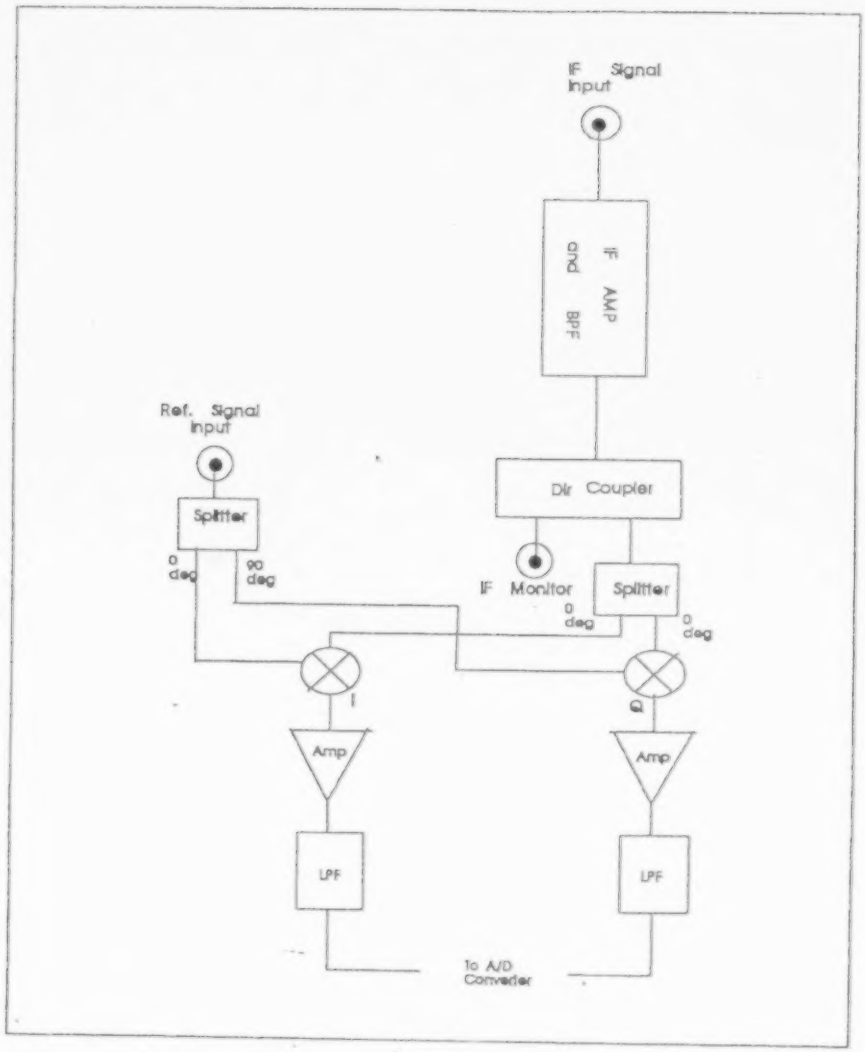

Figure 2.2 A schematic diagram of an IF channel of the multipath measurement system.

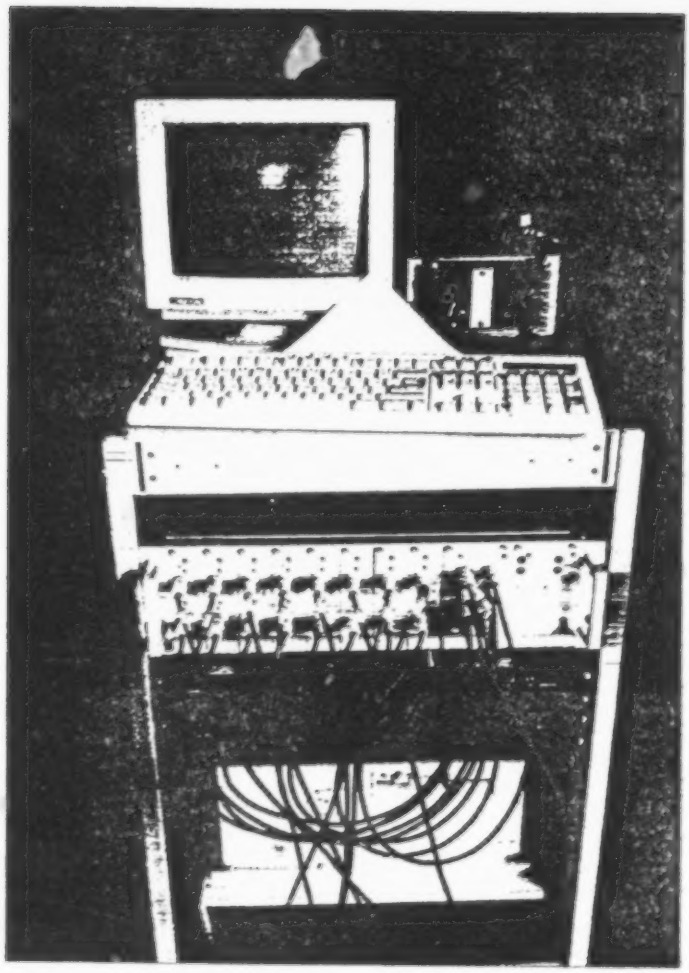

Figure 2.3 The data acquisition unit of the multipath measurement system.

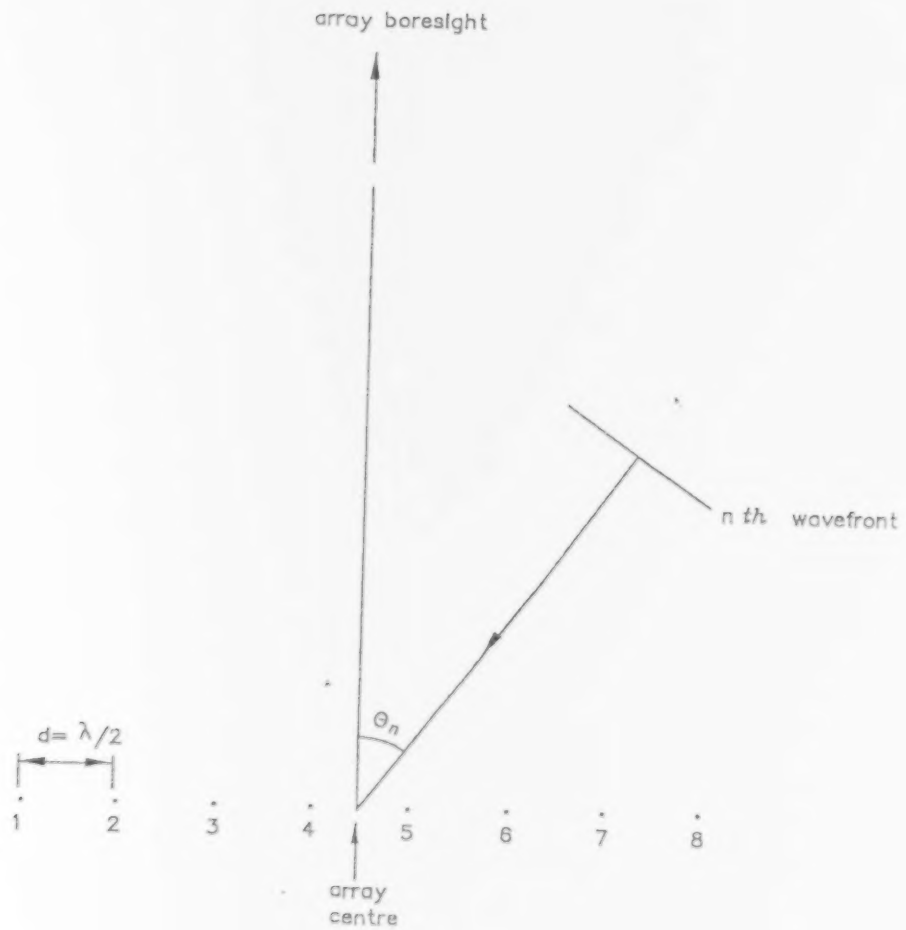

Figure 3.1 Geometry of a linear array, showing a ray of an incident plane wave.

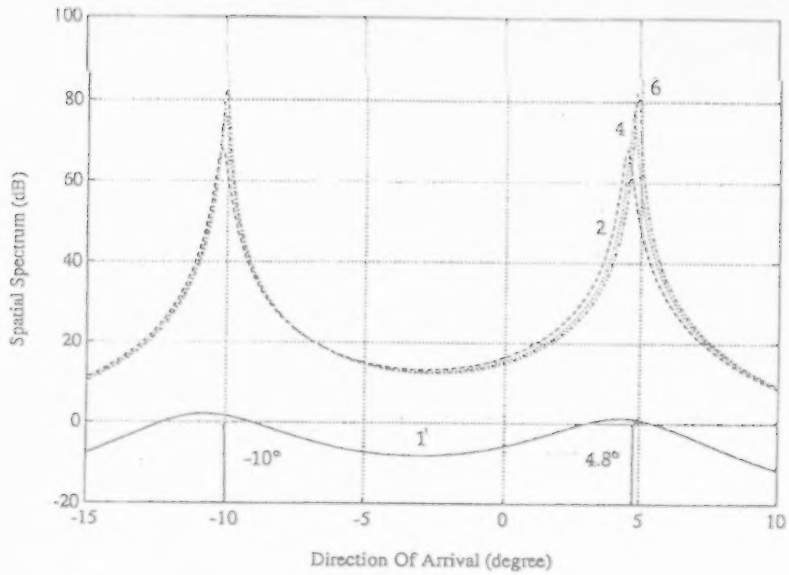

(a) Spatial spectrum after iterations 1, 2, 4, and 6.

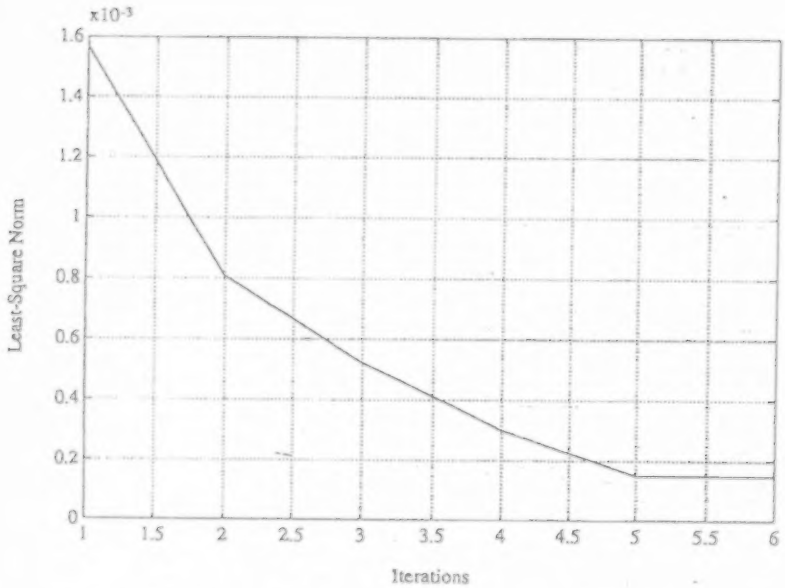

(b) The convergence of the least-square norm after each iteration.

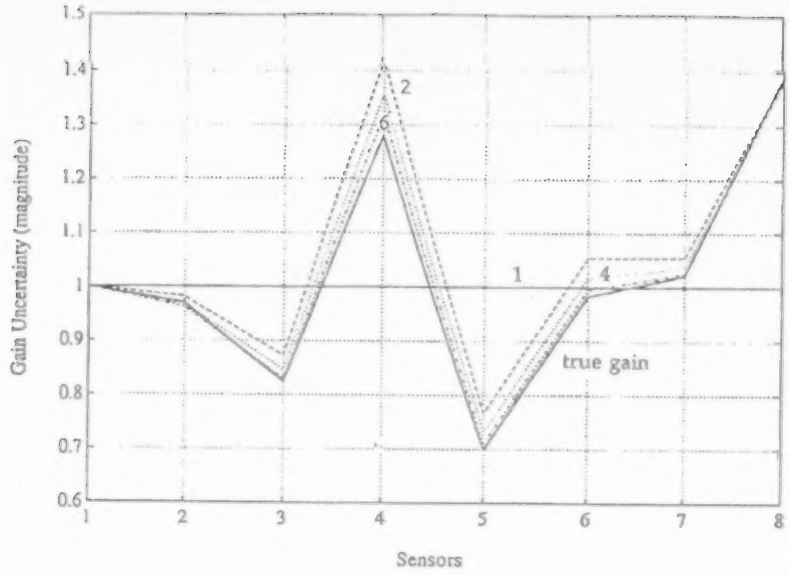

(c) The estimated gain after each iteration.

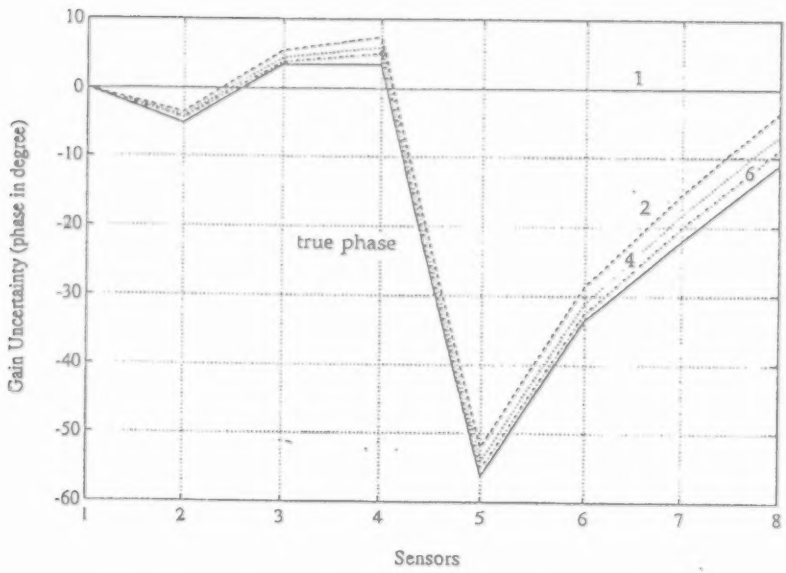

(d) The estimated phase after each iteration.

Figure 4.1 Simulation results based on Ho's calibration algorithm. The input parameters were DOA=(-10°, 5°), gain variance σ_α=0.5, phase variance σ_ψ=20°, SNR=30dB.

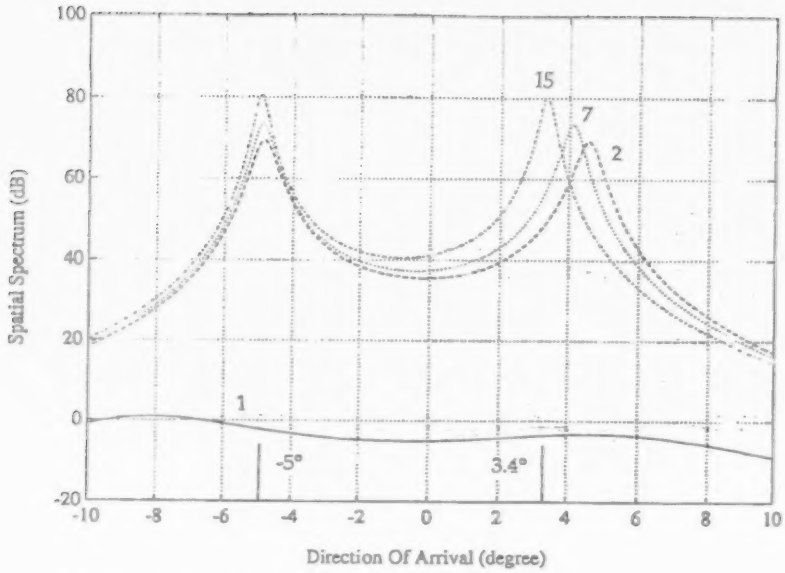

(a) Spatial spectrum after iterations 1, 2, 7, and 15.

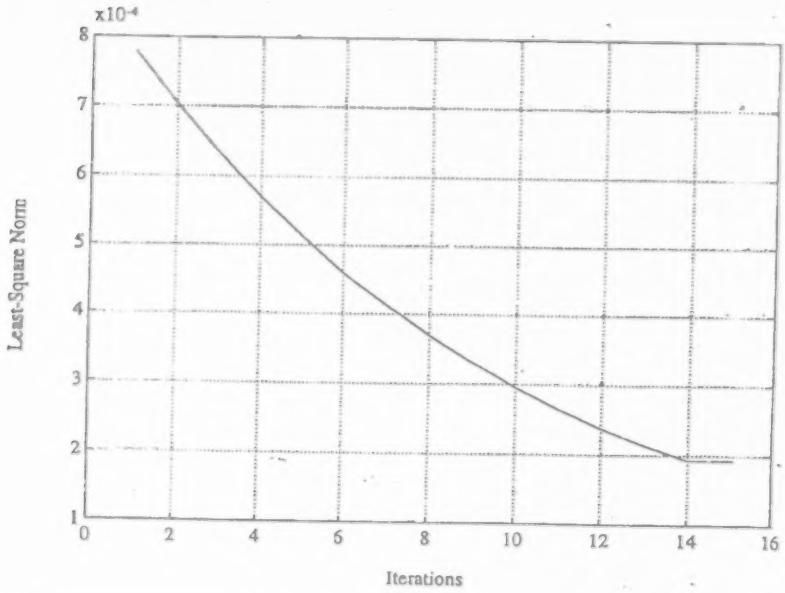

(b) The convergence of the least-square norm after each iteration.

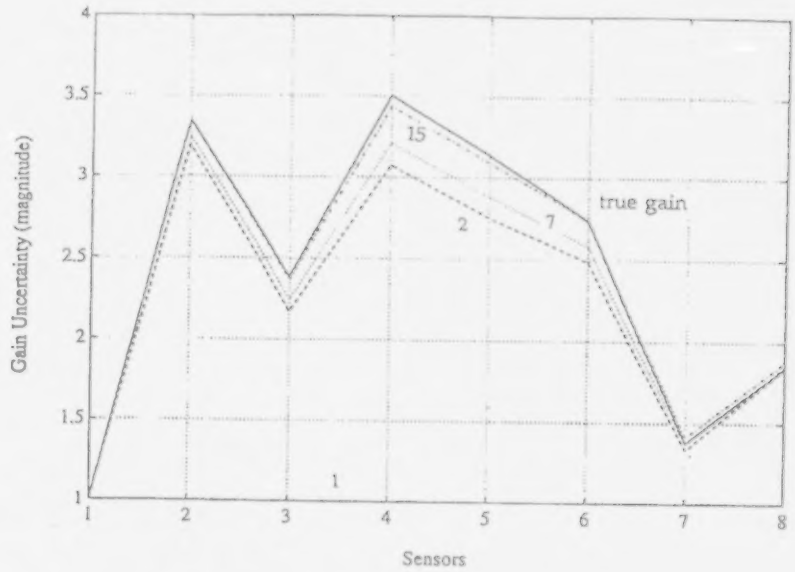

(c) The estimated gain after each iteration.

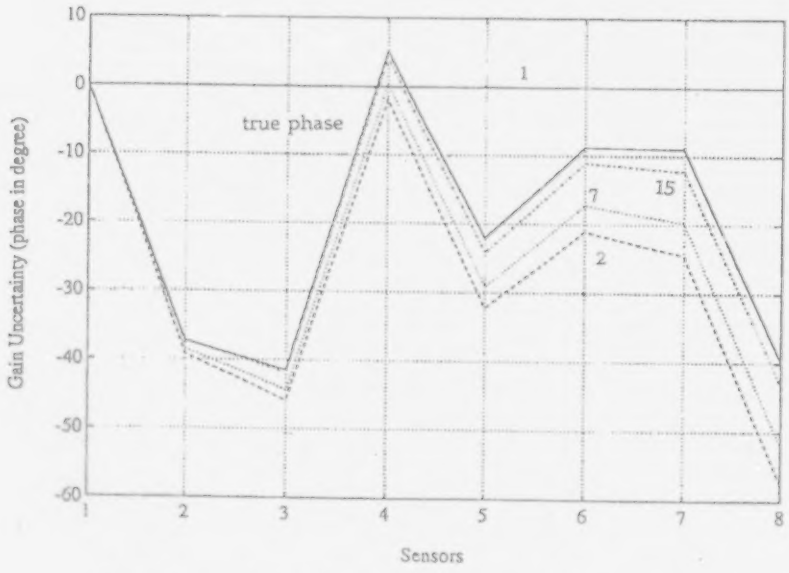

(d) The estimated phase after each iteration.

Figure 4.2 Simulation results based on Ho's calibration algorithm. The input parameters were DOA=(-5°, 3°), gain variance σ_α=0.5, phase variance σ_ψ=20°, SNR=20 dB.

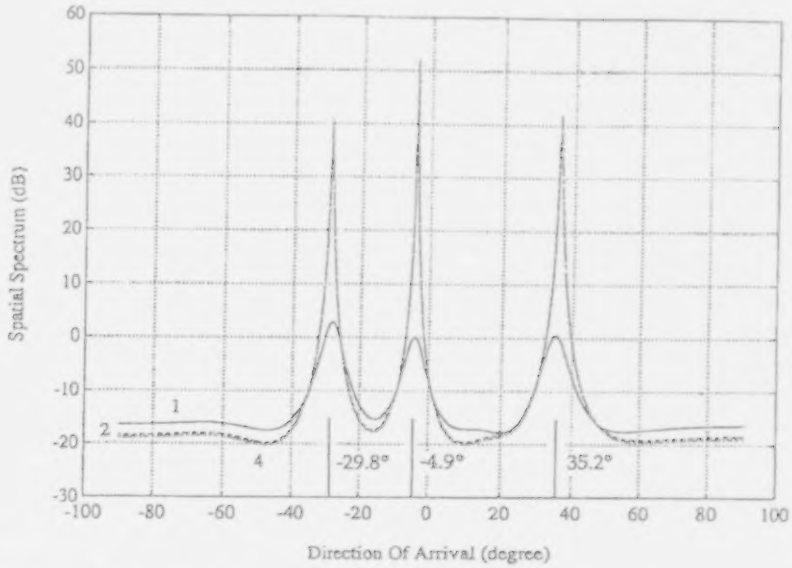

(a) Spatial spectrum after iterations 1, 2, and 4.

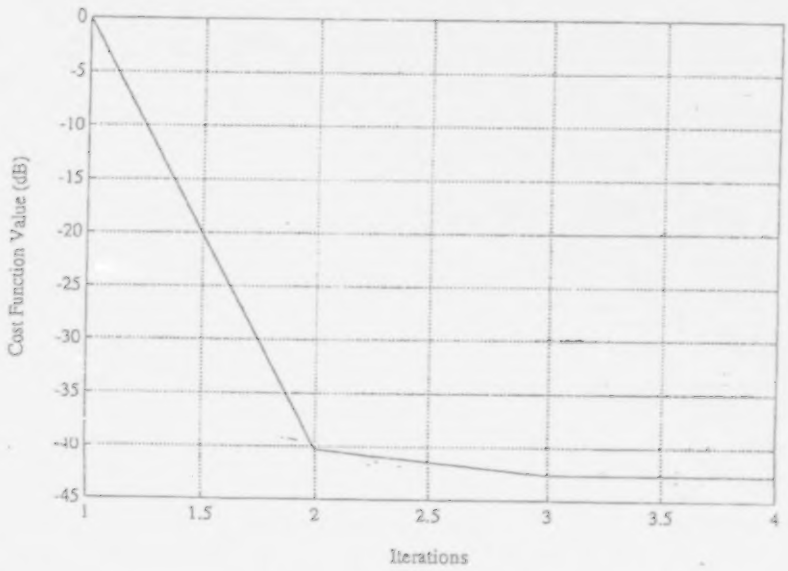

(b) The convergence of the cost function after each iteration.

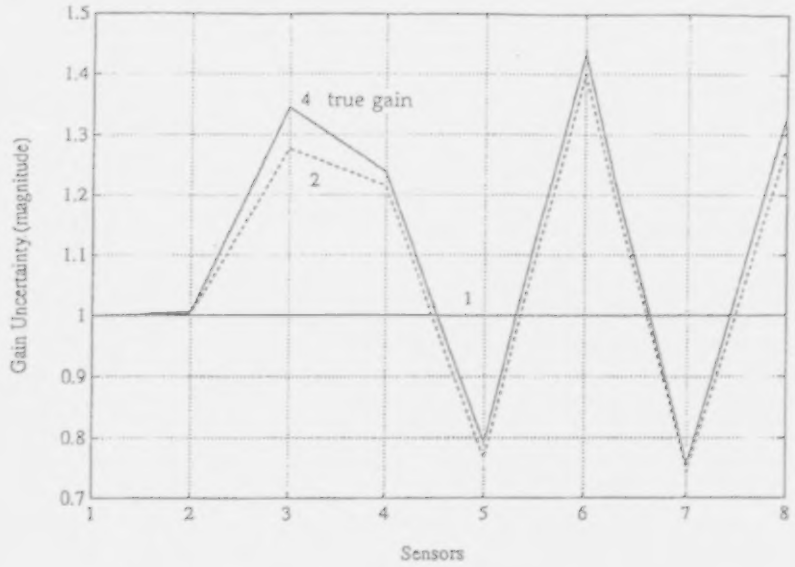

(c) The estimated gain after each iteration.

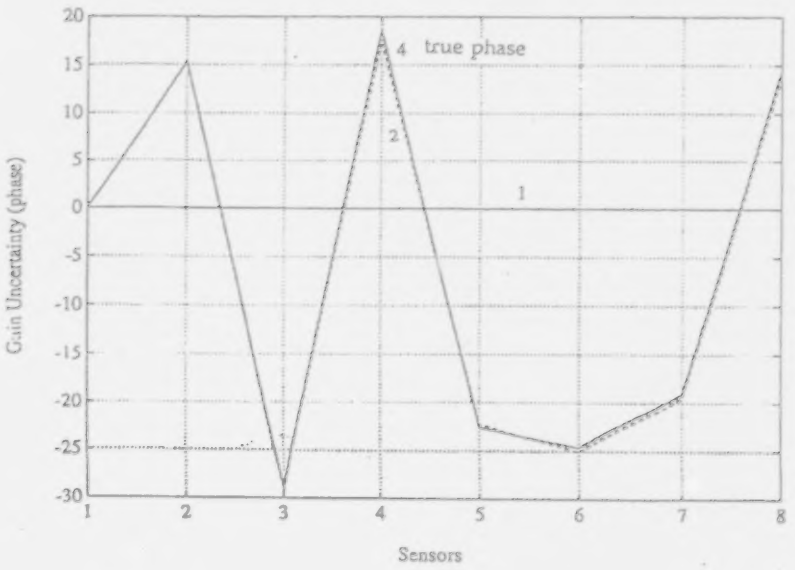

(d) The estimated phase after each iteration.

Figure 4.3 Simulation results based on Friedlander and Weiss's calibration algorithm. The input parameters were DOA=(-30°, -5°, 35°), gain variance σ_α=0.2, phase variance σ_ψ=20°, SNR=20 dB.

P148381.PDF [Page: 62 of 87]

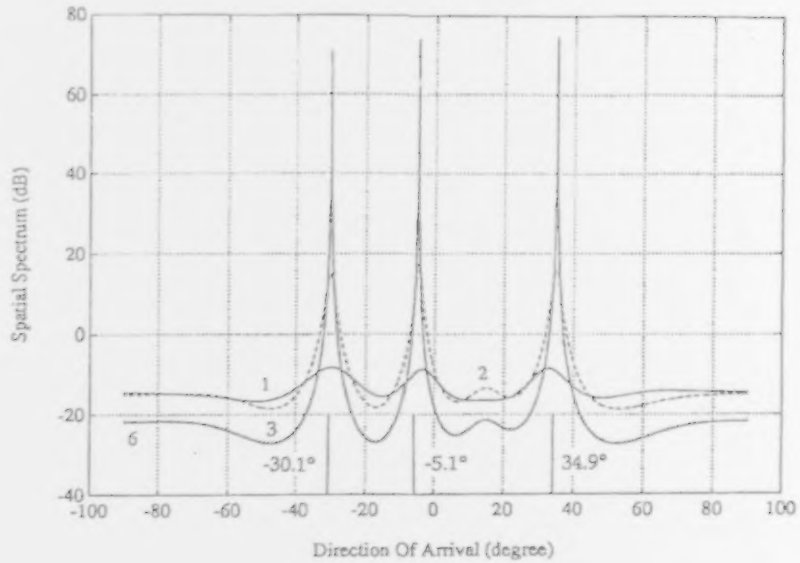

(a) Spatial spectrum after iterations 1, 2, 3, and 6.

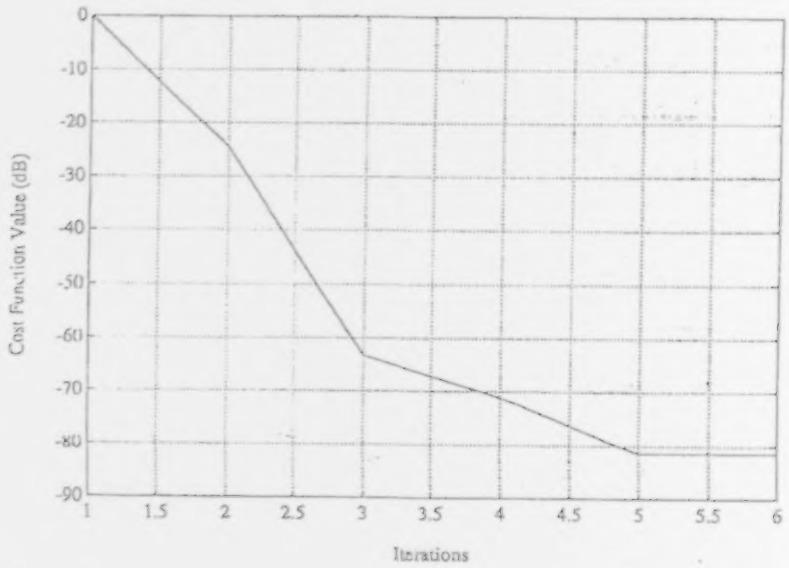

(b) The convergence of the cost function after each iteration.

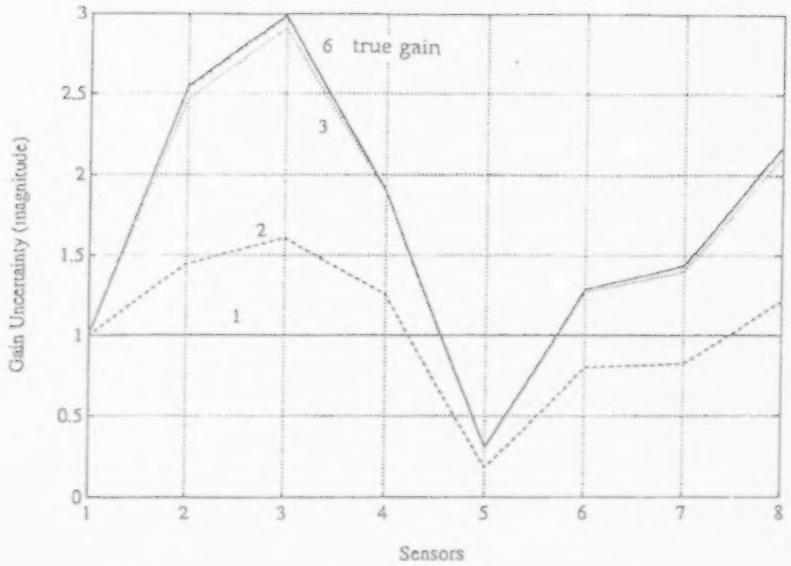

(c) The estimated gain after each iteration.

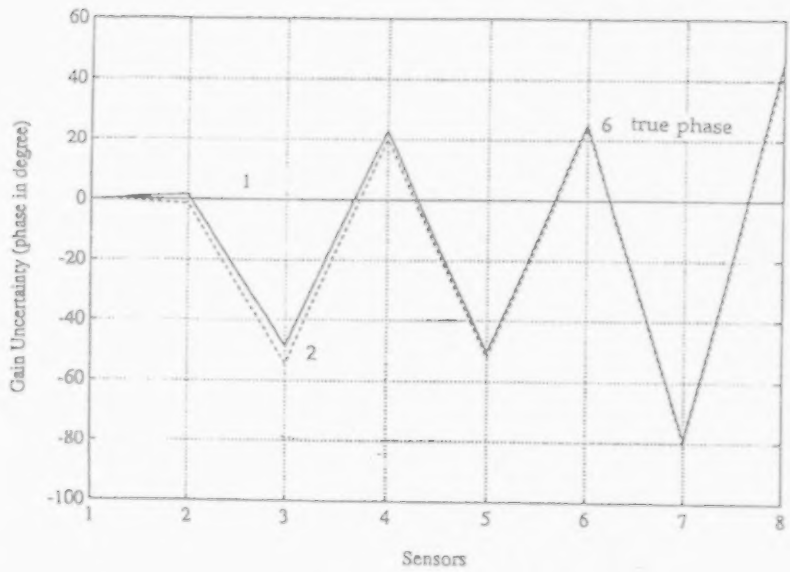

(d) The estimated phase after each iteration.

Figure 4.4 Simulation results based on Friedlander and Weiss's calibration algorithm. The input parameters were DOA=(-30°, -5°, 35°), gain variance σ_α=0.5, phase variance σ_ψ=40°, SNR=30 dB.

P148381.PDF [Page: 64 of 87]

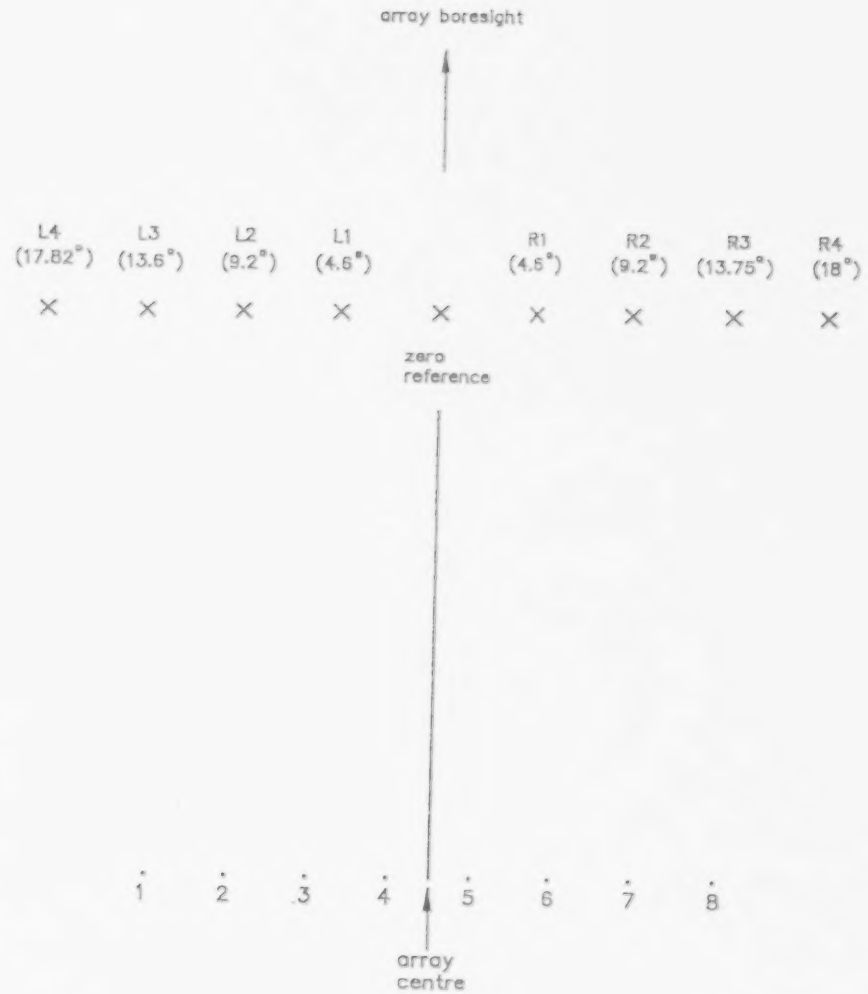

Figure 5.1 A site survey on bearing measurement using a theodolite.

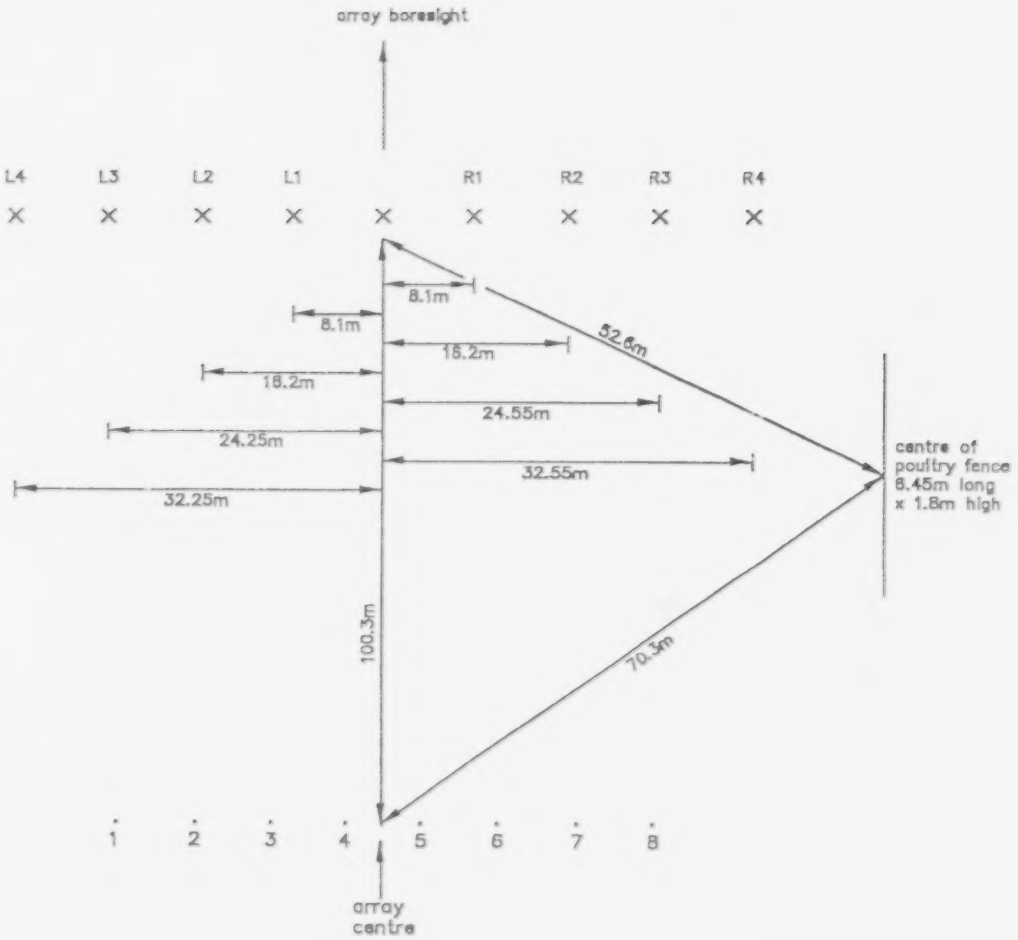

Figure 5.2 A site survey based on tape measurement.

P148381.PDF [Page: 66 of 87]

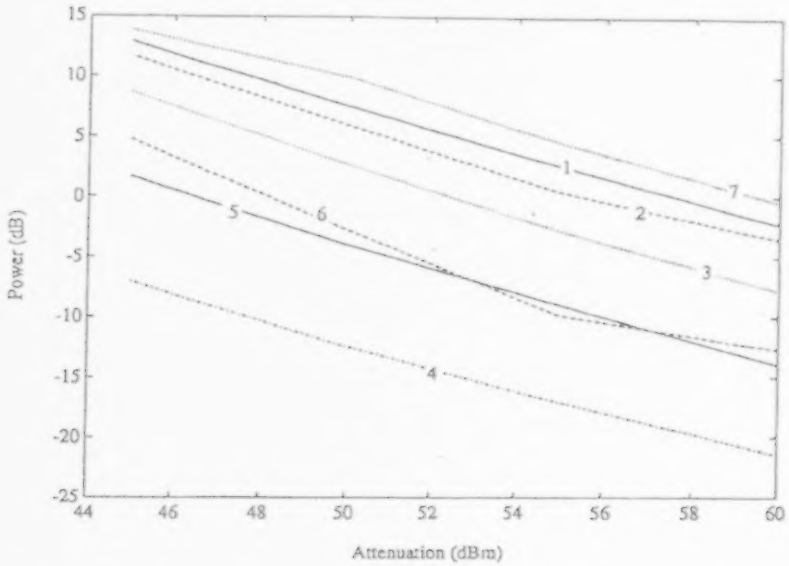

(a) Gain characteristics due to various signal attenuation.

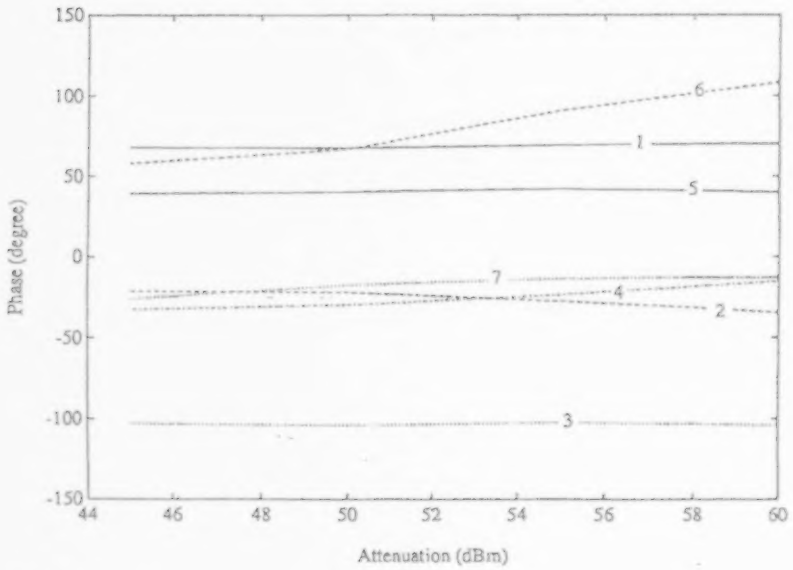

(b) Phase characteristics due to various signal attenuation.

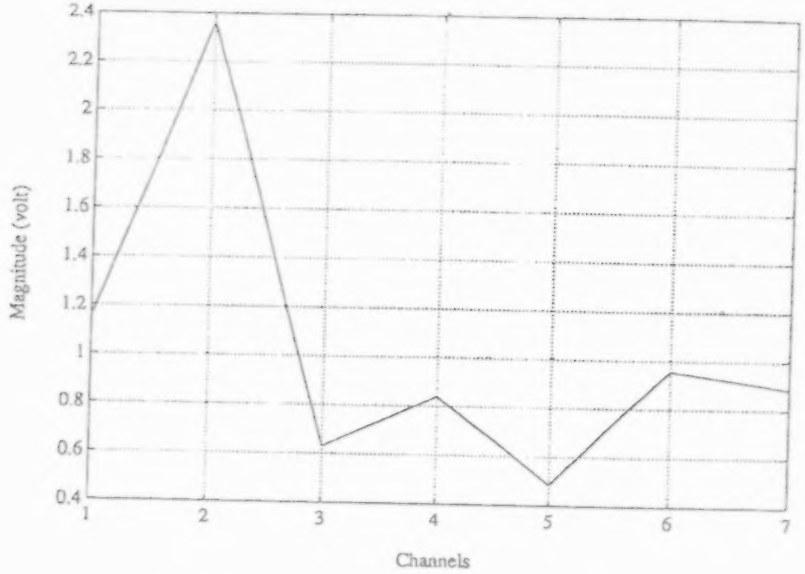

(c) Magnitude of the dc offset value.

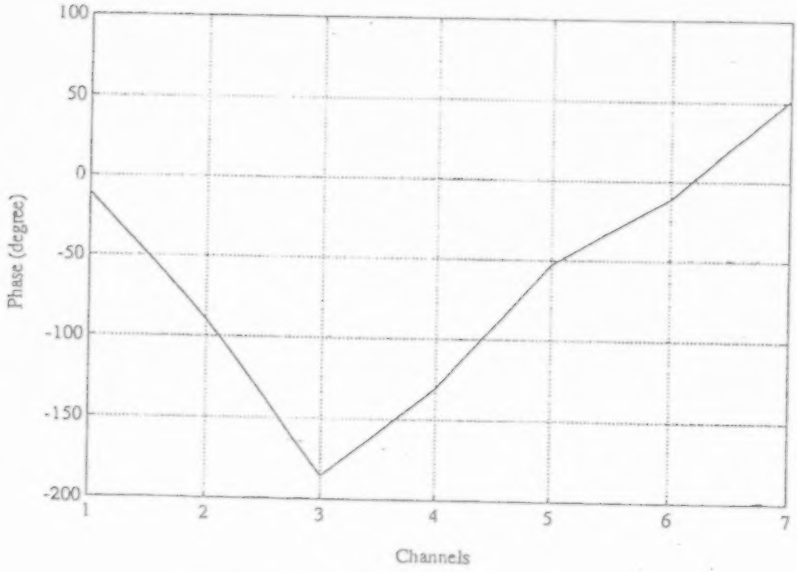

(d) Phase of the dc offset value.

Figure 5.3 System calibration carried out on April 28 am, 1992.

P148381.PDF [Page: 68 of 87]

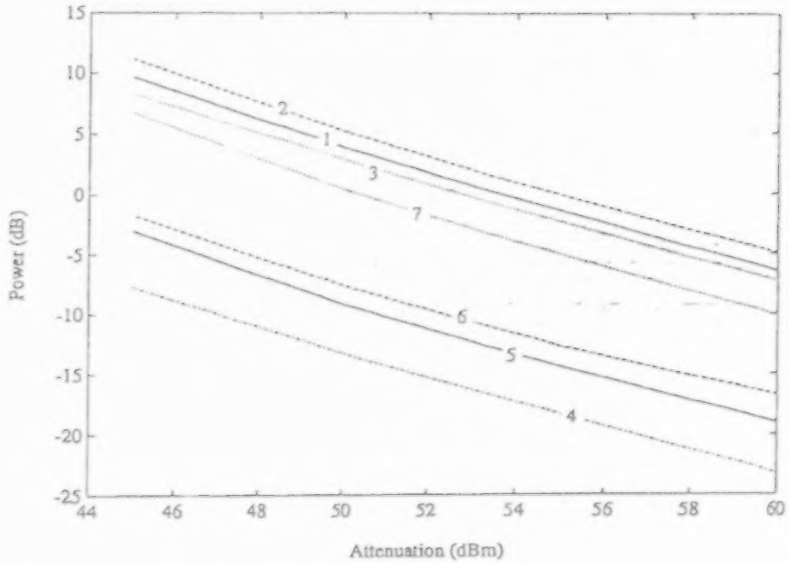

(a) Gain characteristics due to various signal attenuation.

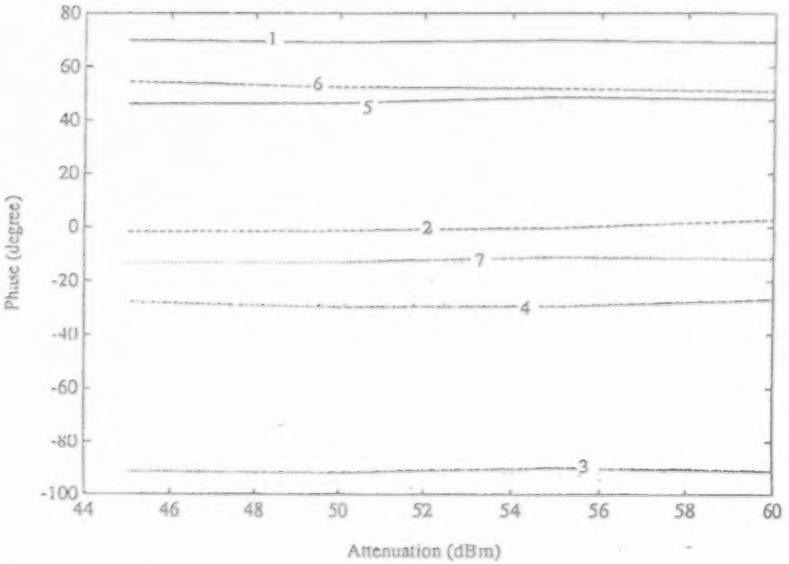

(b) Phase characteristics due to various signal attenuation.

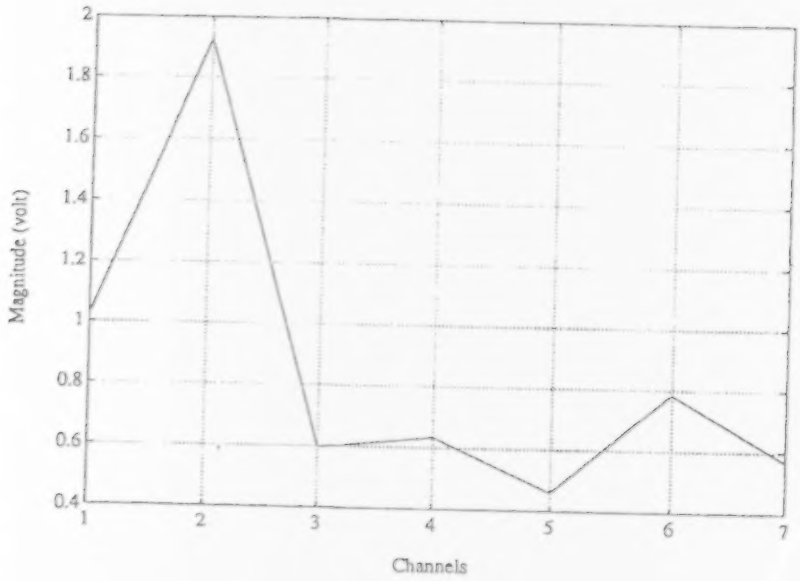

(c) Magnitude of the dc offset value.

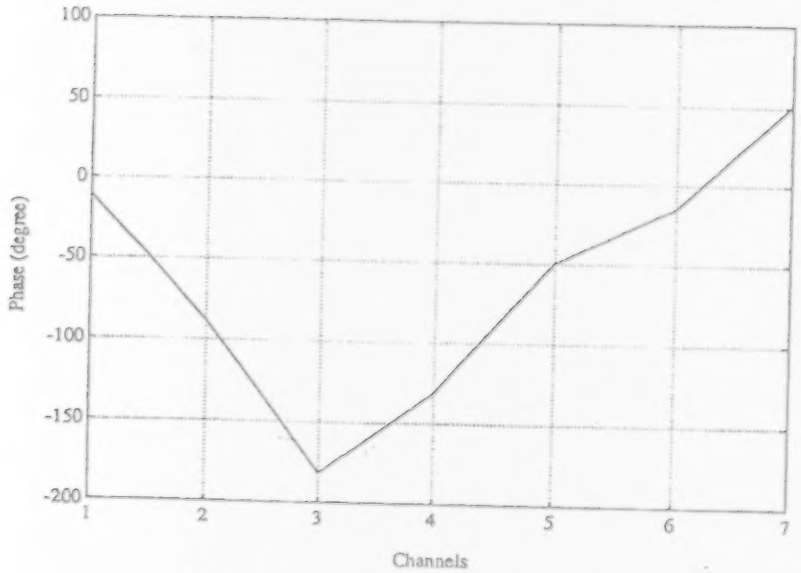

(d) Phase of the dc offset value.

Figure 5.4 System calibration carried out on April 28 pm, 1992.

P148381.PDF [Page: 70 of 87]

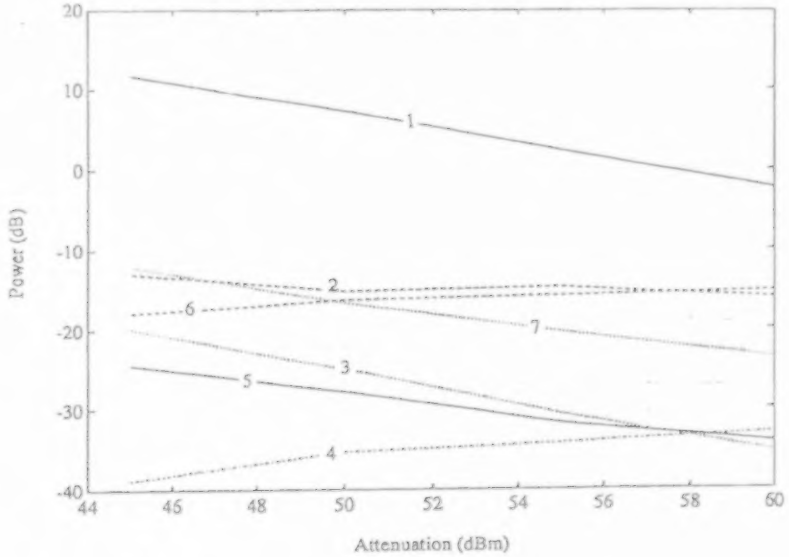

(a) Gain characteristics due to various signal attenuation.

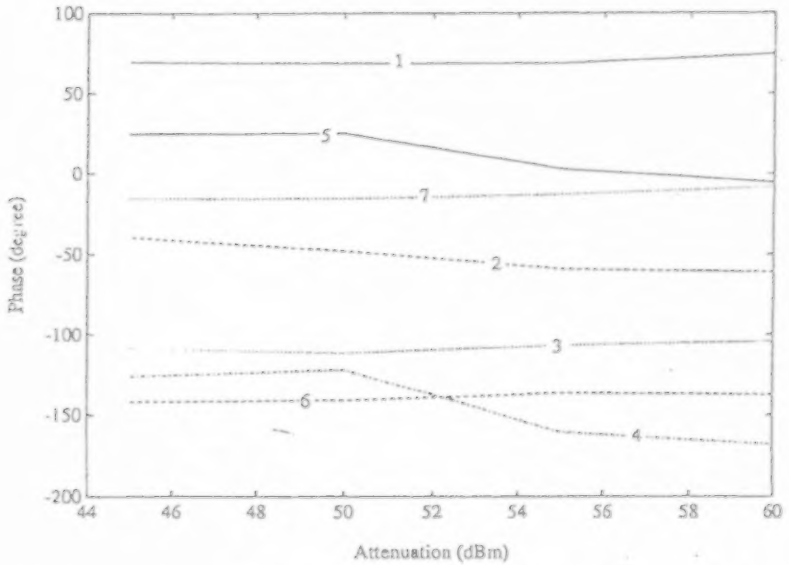

(b) Phase characteristics due to various signal attenuation.

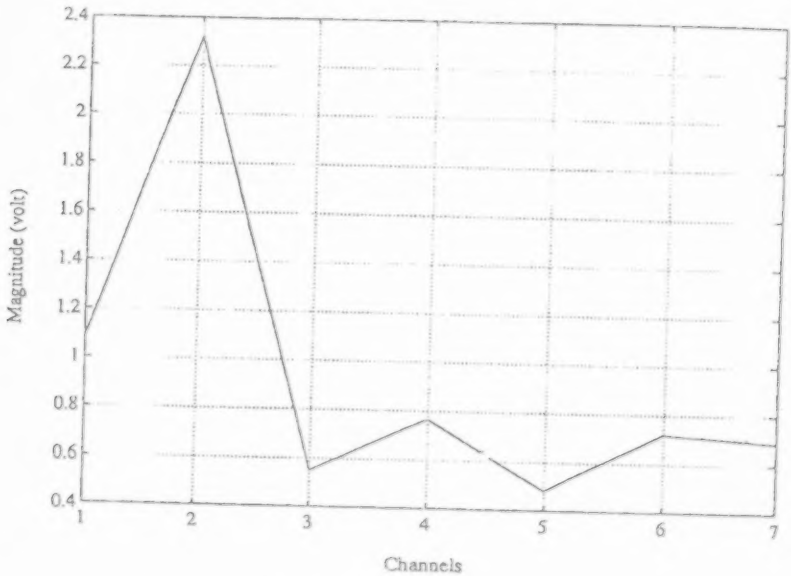

(c) Magnitude of the dc offset value.

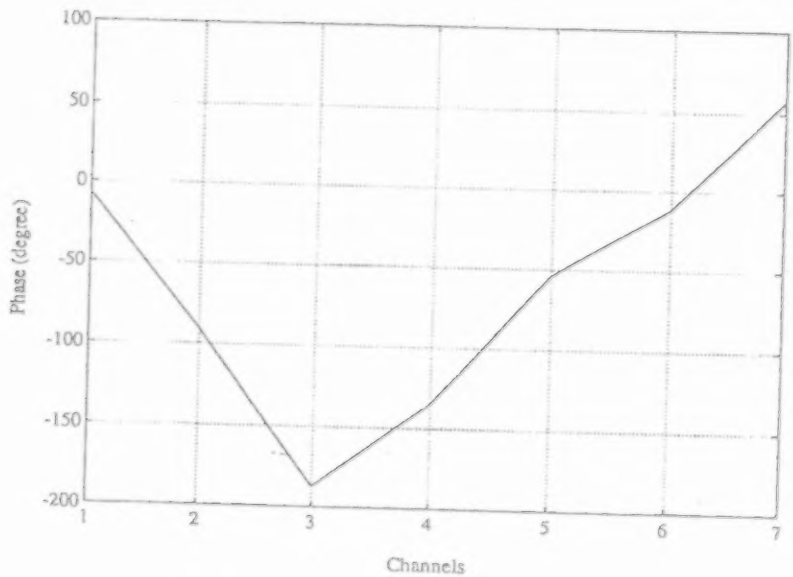

(d) Phase of the dc offset value.

Figure 5.5 System calibration carried out on April 29, 1992.

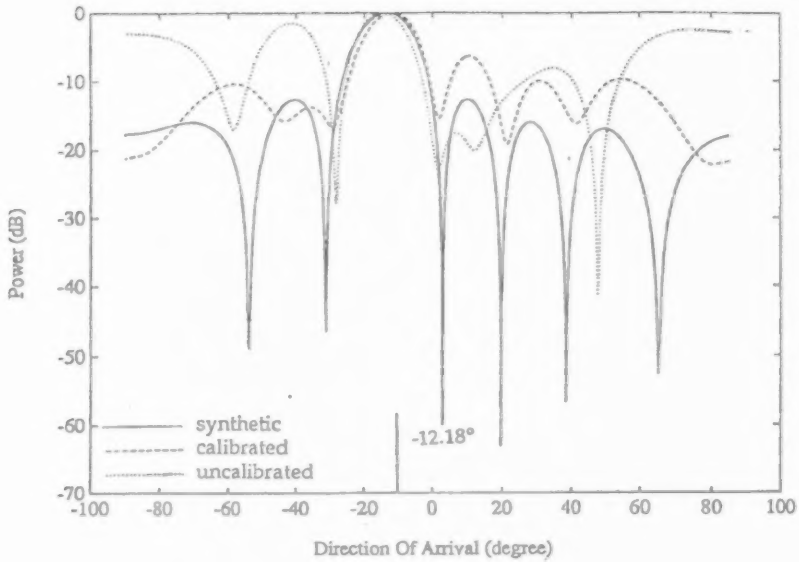

(a) Beam pattern.

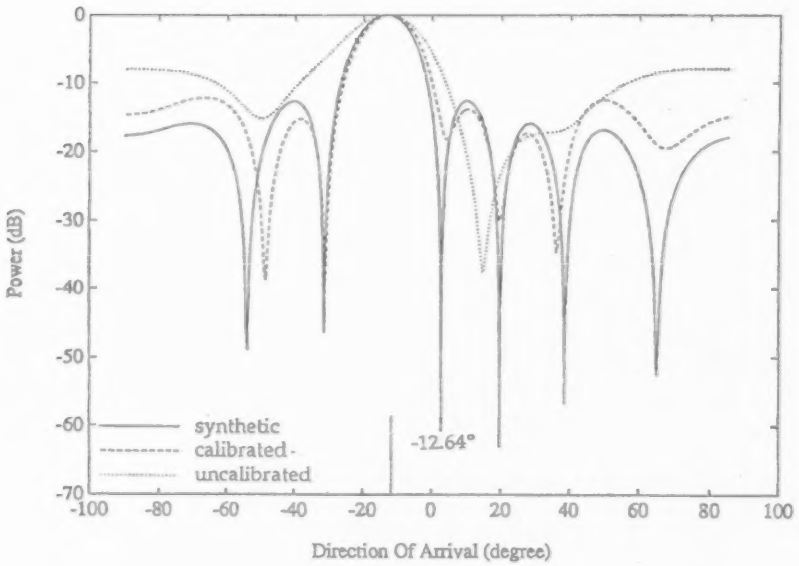

(b) Beam pattern with channel gain imbalance and dc offset removed.

Figure 5.6 FFT beamforming with source at L3, i.e., 13.6° left of the array boresight.

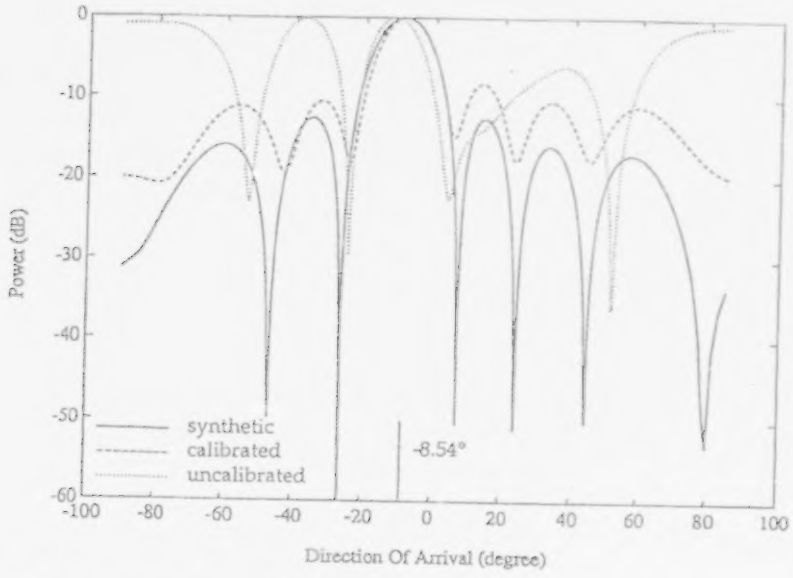

(a) Beam pattern.

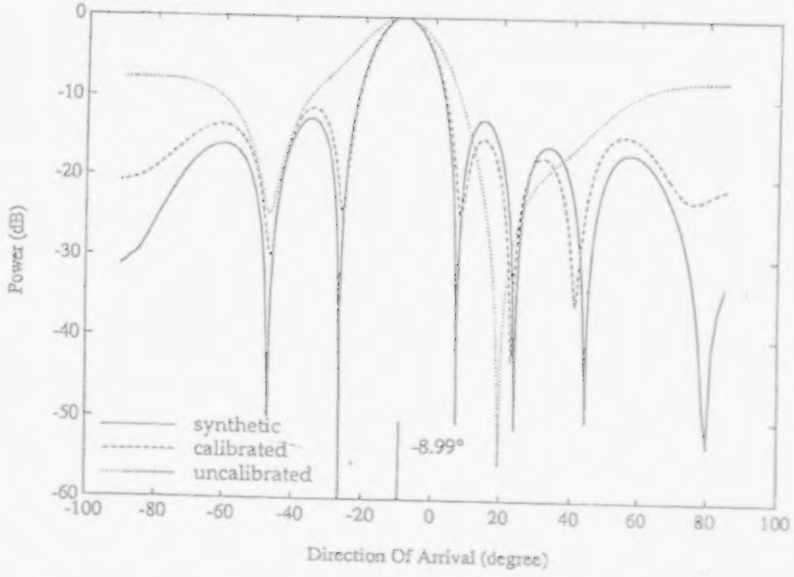

(b) Beam pattern with channel gain imbalance and dc offset removed.

Figure 5.7 FFT beamforming with source at L2, i.e., 9.2° left of the array boresight.

P148381.PDF [Page: 74 of 87]

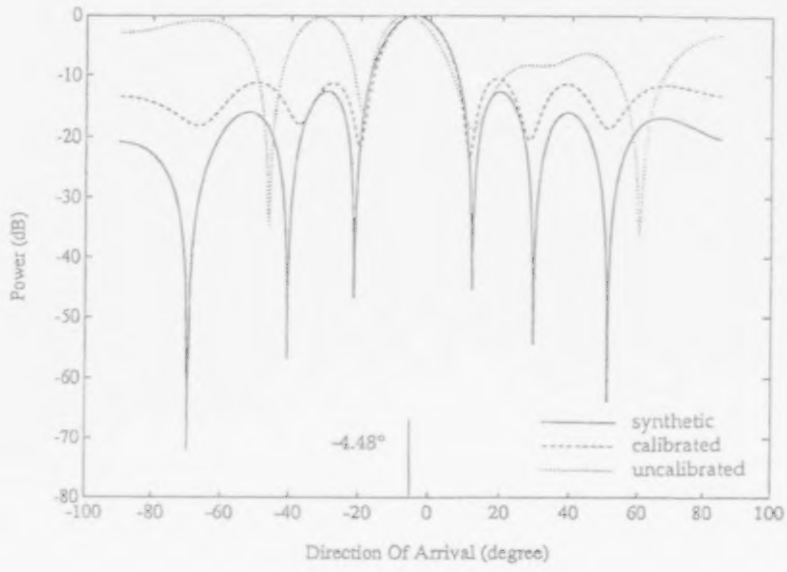

(a) Beam pattern.

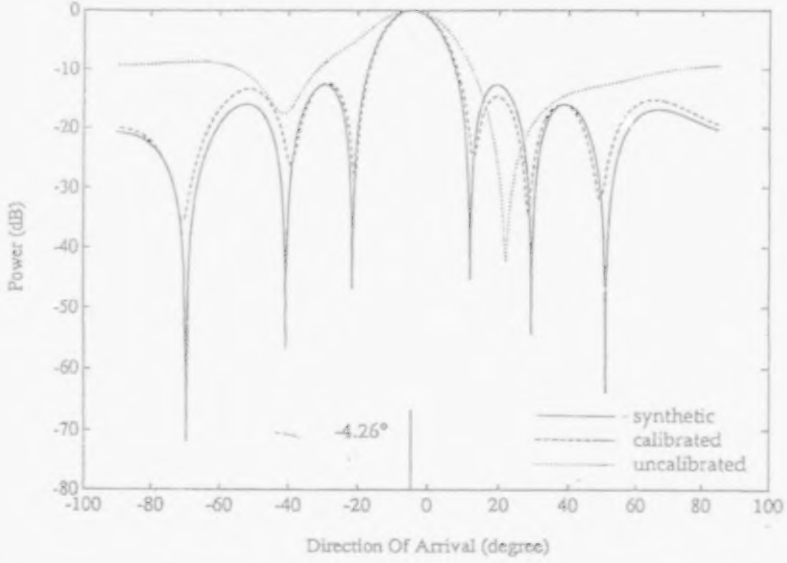

(b) Beam pattern with channel gain imbalance and dc offset removed.

Figure 5.8 FFT beamforming with source at L1, i.e., 4.6° left of the array boresight.

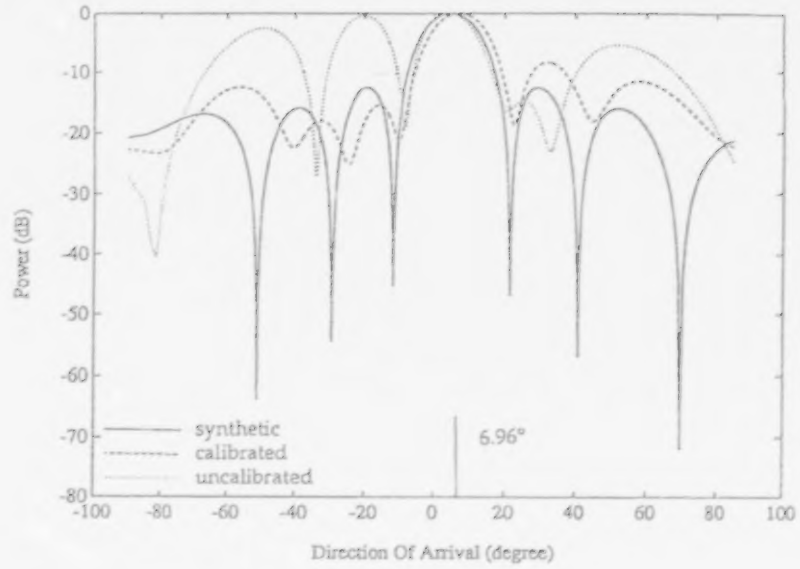

(a) Beam pattern.

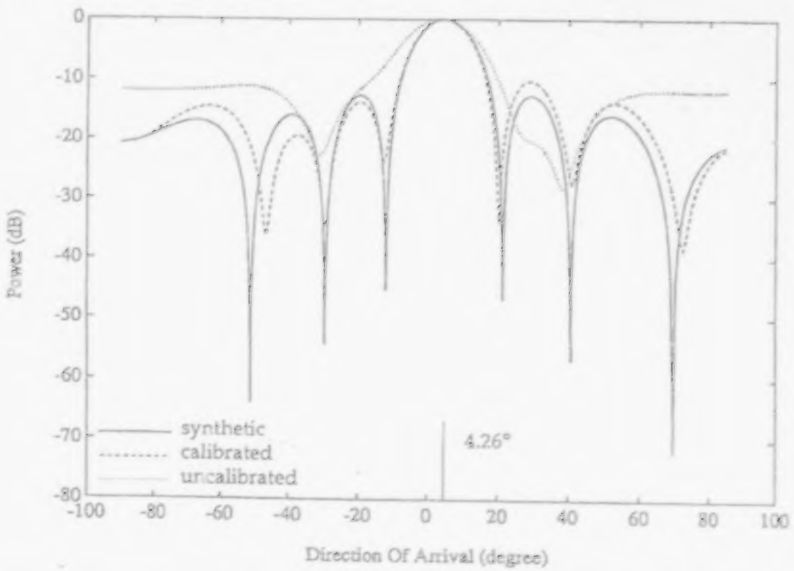

(b) Beam pattern with channel gain imbalance and dc offset removed.

Figure 5.9 FFT beamforming with source at R1, i.e., 4.6° right of the array boresight.

P148381.PDF [Page: 76 of 87]

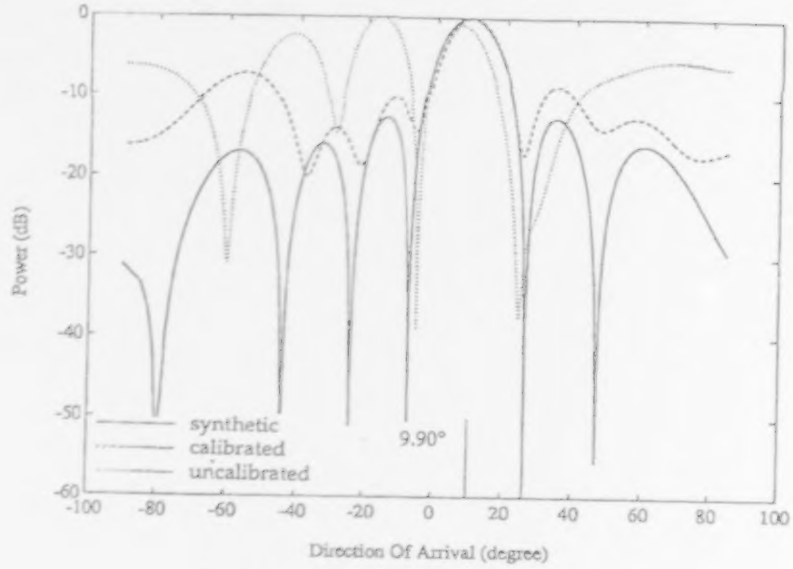

(a) Beam pattern.

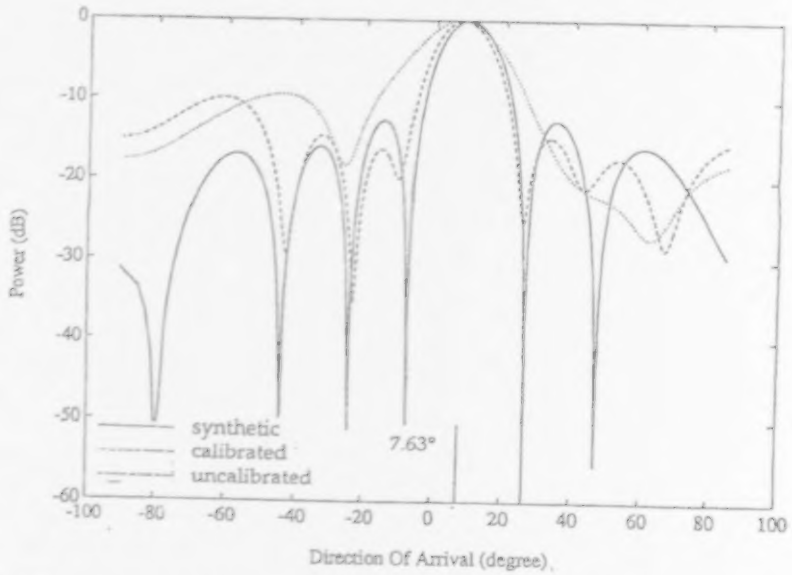

(b) Beam pattern with channel gain imbalance and dc offset removed.

Figure 5.10 FFT beamforming with source at R2, i.e., 9.2° right of the array boresight.

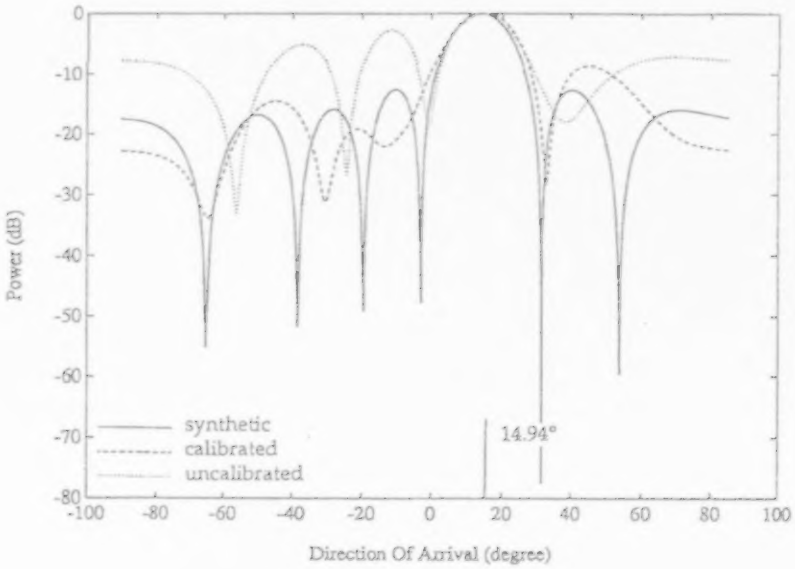

(a) Beam pattern.

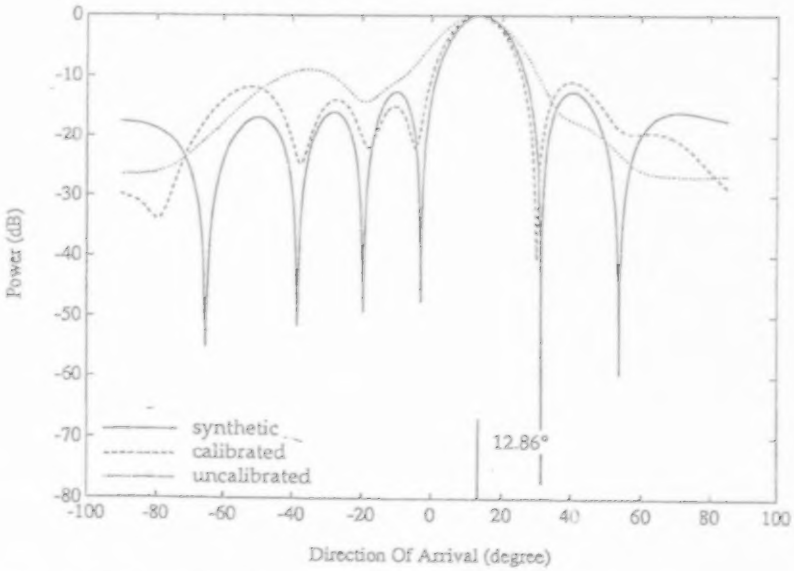

(b) Beam pattern with channel gain imbalance and dc offset removed.

Figure 5.11 FFT beamforming with source at R3, i.e., 13.75° right of the array boresight.

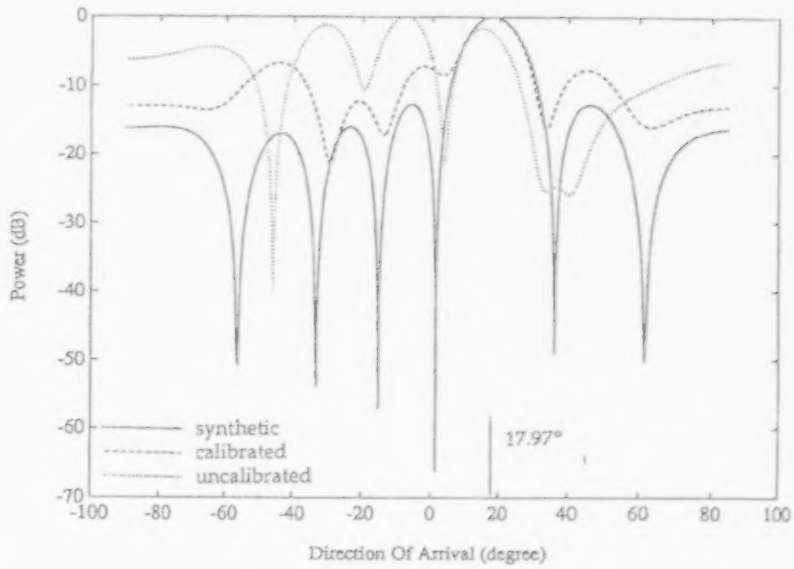

(a) Beam pattern.

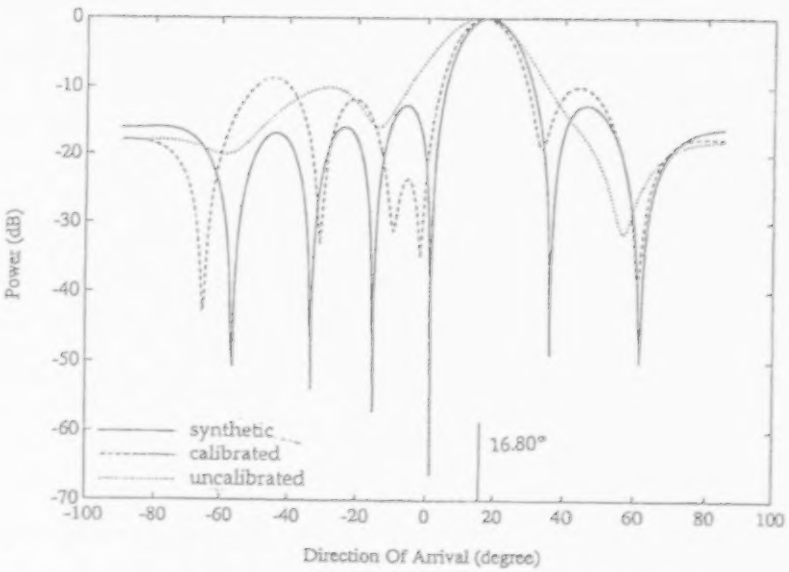

(b) Beam pattern with channel gain imbalance and dc offset removed.

Figure 5.12 FFT beamforming with source at R4, i.e., 18° right of the array boresight.

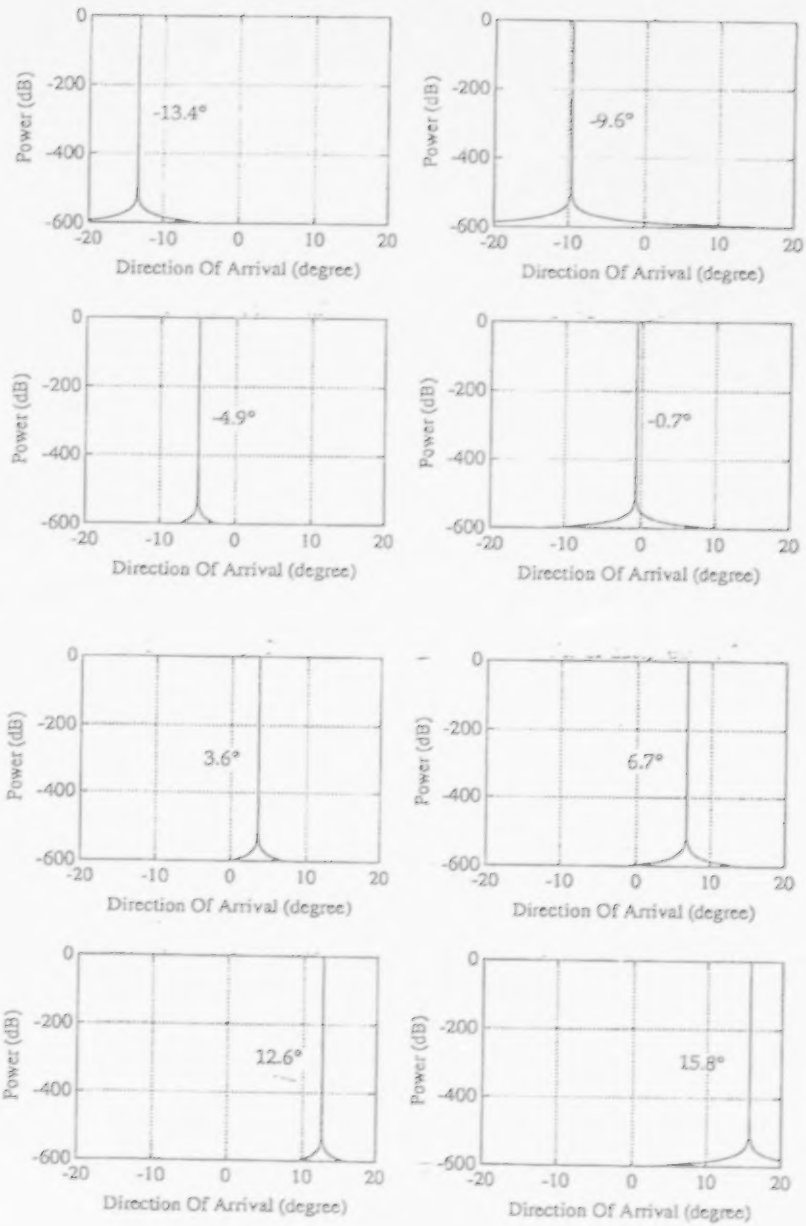

Figure 5.13 Direction of arrival estimation on real data using Friedlander and Weiss's calibration algorithm.

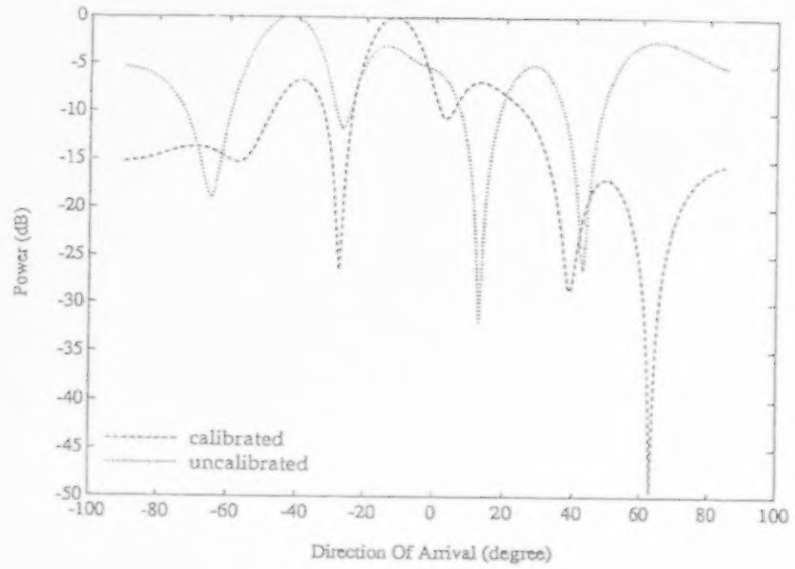

(a) Beam pattern.

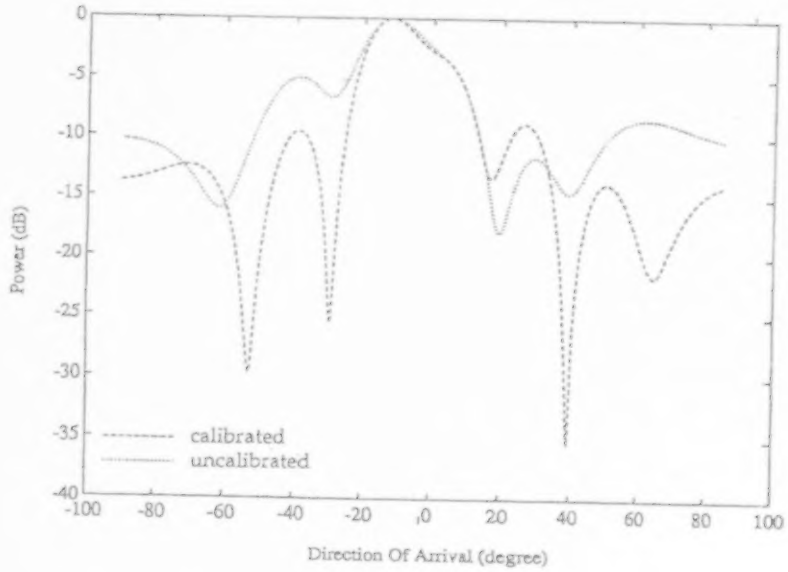

(b) Beam pattern with channel gain imbalance and dc offset removed.

Figure 5.14 FFT beamforming on two coherent sources. Sources were at -9.2° and 0°.

P148381.PDF [Page: 81 of 87]

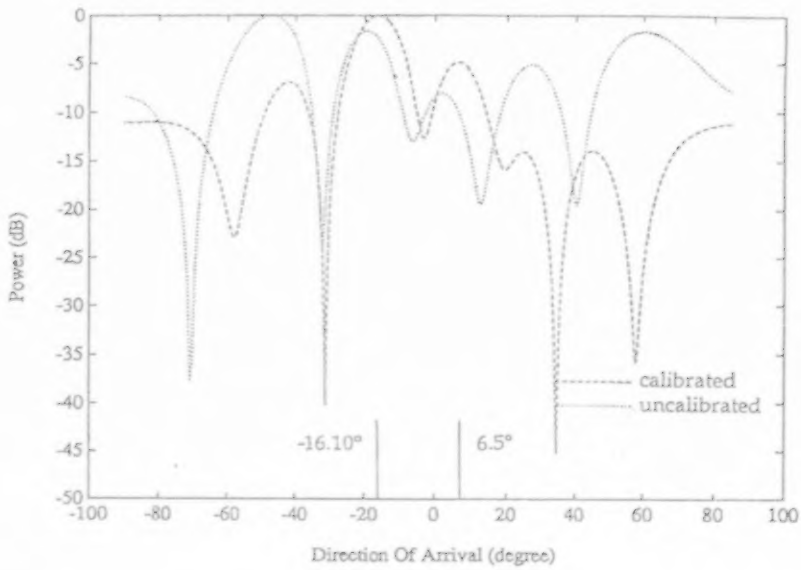

(a) Beam pattern.

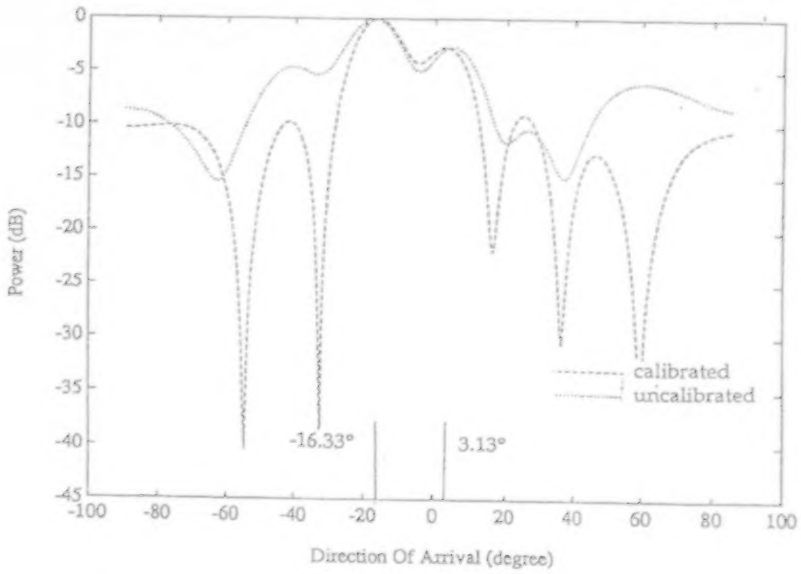

(b) Beam pattern with channel gain imbalance and dc offset removed.

Figure 5.15 FFT beamforming on two coherent sources. Sources were at -13.6° and 0°.

P148381.PDF [Page: 82 of 87]

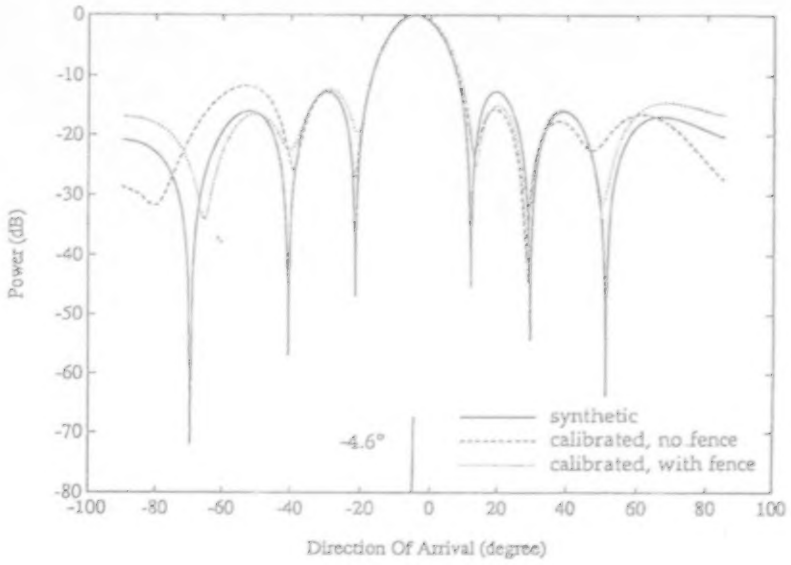

Figure 5.16 FFT beamforming pattern with the presence of a poultry fence. The source was at -4.6° with respect to the array boresight.

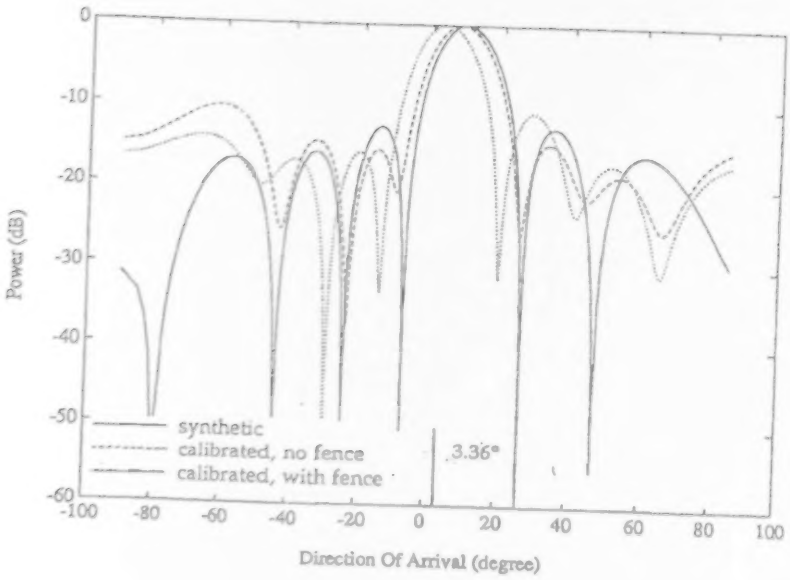

Figure 5.17 FFT beamforming pattern with the presence of a poultry fence. The source was at 9.2° with respect to the array boresight.

P148381.PDF [Page: 84 of 87]

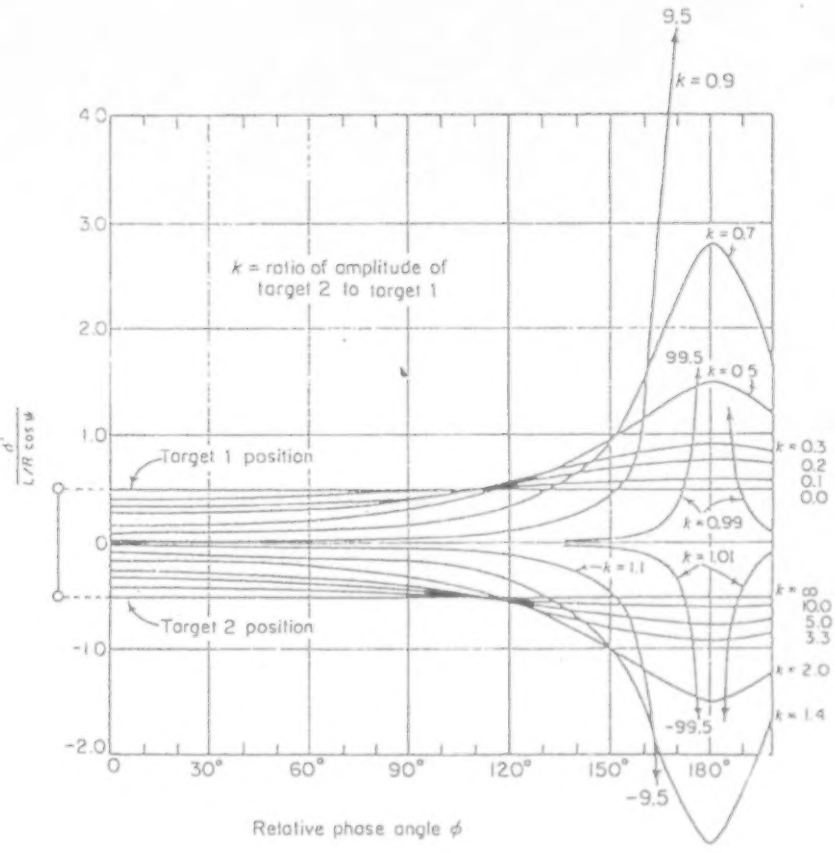

Figure 5.18 Glint for the two-element target [6].

UNCLASSIFIED

SECURITY CLASSIFICATION OF FORM
(highest classification of Title, Abstract, Keywords)

DOCUMENT CONTROL DATA

(Security classification of title, body of abstract and indexing annotation must be entered when the overall document is classified)

1. ORIGINATOR (the name and address of the organization preparing the document. Organizations for whom the document was prepared, e.g. Establishment sponsoring a contractor's report, or tasking agency, are entered in section 8.)

COMMUNICATIONS RESEARCH LABORATORY
MCMASTER UNIVERSITY
HAMILTON, ONTARIO CANADA

2. SECURITY CLASSIFICATION (overall security classification of the document, including special warning terms if applicable)

UNCLASSIFIED

3. TITLE (the complete document title as indicated on the title page. Its classification should be indicated by the appropriate abbreviation (S,C or U) in parentheses after the title.)

MULTIPATH MEASUREMENT AND MODELLING (U)

4. AUTHORS (Last name, first name, middle initial)

LITVA, JOHN AND LAI, L.

5. DATE OF PUBLICATION (month and year of publication of document)

JULY 1992

6a. NO. OF PAGES (total containing information. Include Annexes, Appendices, etc.)

62

6b. NO. OF REFS (total cited in document)

6

7. DESCRIPTIVE NOTES (the category of the document, e.g. technical report, technical note or memorandum. If appropriate, enter the type of report, e.g. interim, progress, summary, annual or final. Give the inclusive dates when a specific reporting period is covered.)

FINAL CONTRACTOR REPORT

8. SPONSORING ACTIVITY (the name of the department project office or laboratory sponsoring the research and development. Include the address.)

DEFENCE RESEARCH ESTABLISHMENT OTTAWA
NATIONAL DEFENCE
SHIRLEY BAY, OTTAWA, ONTARIO K1A 0K2 CANADA

9a. PROJECT OR GRANT NO. (if appropriate, the applicable research and development project or grant number under which the document was written. Please specify whether project or grant)

041LX

9b. CONTRACT NO. (if appropriate, the applicable number under which the document was written)

W7714-1-9507

10a. ORIGINATOR'S DOCUMENT NUMBER (the official document number by which the document is identified by the originating activity. This number must be unique to this document.)

DREO DRP 93-636

10b. OTHER DOCUMENT NOS. (Any other numbers which may be assigned this document either by the originator or by the sponsor)

11. DOCUMENT AVAILABILITY (any limitations on further dissemination of the document, other than those imposed by security classification)

(X) Unlimited distribution
( ) Distribution limited to defence departments and defence contractors; further distribution only as approved
( ) Distribution limited to defence departments and Canadian defence contractors; further distribution only as approved
( ) Distribution limited to government departments and agencies; further distribution only as approved
( ) Distribution limited to defence departments; further distribution only as approved
( ) Other (please specify):

12. DOCUMENT ANNOUNCEMENT (any limitation to the bibliographic announcement of this document. This will normally correspond to the Document Availabilty (11). However, where further distribution (beyond the audience specified in 11) is possible, a wider announcement audience may be selected.)

UNLIMITED

UNCLASSIFIED
SECURITY CLASSIFICATION OF FORM

13. ABSTRACT (a brief and factual summary of the document. It may also appear elsewhere in the body of the document itself. It is highly desirable that the abstract of classified documents be unclassified. Each paragraph of the abstract shall begin with an indication of the security classification of the information in the paragraph (unless the document itself is unclassified) represented as (S), (C), or (U). It is not necessary to include here abstracts in both offical languages unless the text is bilingual).

(U) This report is part of ongoing work being carried out to study the effects of multipath on a direction finding (DF) system. An advanced eight-element DF system has been developed based on digital beamforming technology. The system was used to collect field trial data. The measurement trials included system calibration, single-source and two-source measurements, and measurements in the presence of specular multipath environment generated by a known object. A database was established, on which the analysis of the multipath effects was based.

(U) A number of data calibration techniques have been investigated. ~~They included:~~ Ho's array calibration algorithm, Friedlander-Weiss's self calibration algorithm, and calibration based on reference data. ~~It was found that~~ Ho's technique exhibited a slow rate of convergence. Friedlander-Weiss's technique gives good estimates and converges at a faster rate. ~~It was also found that~~ the third calibration method produced accurate estimates.

(U) A preliminary analysis of the data was carried out. For single source, DOA estimates showed very good accuracy. ~~As well,~~ the beam patterns were seen to be reasonably close to those predicted theoretically. A large deviation in DOA was observed in the presence of specular multipath. It is believed that this effect was caused by the glint phenomena.

(U) Based on the observations and findings during the course of this work, a number of recommendations are made for future research.

14. KEYWORDS, DESCRIPTORS or IDENTIFIERS (technically meaningful terms or short phrases that characterize a document and could be helpful in cataloguing the document. They should be selected so that no security classification is required. Identifiers, such as equipment model designation, trade name, military project code name, geographic location may also be included. If possible keywords should be selected from a published thesaurus. e.g. Thesaurus of Engineering and Scientific Terms (TEST) and that thesaurus-identified. If it is not possible to select indexing terms which are Unclassified, the classification of each should be indicated as with the title.)

DIRECTION FINDING
VHF
MULTIPATH
CALIBRATION
SELF-CALIBRATION
DIGITAL BEAMFORMING
LINEAR ANTENNA ARRAY
FFT BEAMFORMING